



**POLITECNICO
DI TORINO**

CORSO DI LAUREA MAGISTRALE IN INGEGNERIA AEROSPAZIALE

TESI DI LAUREA MAGISTRALE

Design of a Low Order Model for Flexible Aircraft

Relatore:

Prof. Giorgio Guglieri

Co-Relatore:

Dott.ssa Elisa Capello

Candidato:

Simone Malisani

Aprile 2020

*A mamma, papà, i nonni e Luca
Per aver sempre creduto nei miei sogni
Anche quando io non riuscivo a crederci*

*A Raul, Riccardo, Edoardo, Sofia e Federico
Perché non è importante la meta, ma il cammino
E il sostegno di chi viaggia affianco a te*

*Ai miei coinquilini, passati e presenti
Per avermi insegnato che convivere
È molto più che condividere le mura di casa*

*Ai compagni del Team 1
Per quanto di bello si può costruire in poco
Se accanto hai le persone giuste*

*A tutti gli amici di Bertiole
Perché non importa dove vada
Con voi sono sempre a casa*

*E a tutti quelli che si sono fatti un pezzo di questo viaggio
Condividendo, arricchendo e contribuendo a tracciarne il sentiero
Senza mai prendersene il merito*

Grazie.

Abstract

The changes on aircraft structures and the increased use of advanced and light materials have led to the design of more efficient and flexible aircraft. This implies that rigid body dynamics are no longer sufficient to describe the aircraft behaviour in atmospheric flight. Furthermore, the frequencies of the lower structural modes are close to the frequencies of the rigid aircraft dynamics and, thus, a possible coupling between structural dynamics and piloting task must be taken in consideration during aircraft modelling.

In this thesis, an analytical method, based on a mixed Newtonian-Lagrangian approach, is used to derive a simplified model of the flexible aircraft which maintains a "strong" link with the rigid aircraft equations of motion. Moreover, flexible displacements and torsional variables, starting from the Lagrange's equations, are discretized from the beginning by means of the Galérkin method, i.e. by means of a finite number of generalized coordinates. This approach allows to derive directly a finite-order system of ordinary differential equations, making it less complex and suitable for real time simulation and control law synthesis.

Once the flexible model is defined, a proper gust model must be applied to evaluate the aircraft response. In this work both discrete and continuous gust models are presented, in order to both generate large rigid aircraft loads and excite the elastic modes of the structure. The models here considered are based on continuous random turbulence theory and, thus, a prior introduction to probability and Power Spectral Density (PSD) methods is given. Finally, the implementation of Dryden and von Kármán continuous turbulence models is addressed, since these models are the most used in aircraft design.

So, the aircraft response to a gust can be evaluated, both in terms of deformation variables and dynamic loads, generated on the structure. Two methods of load determination are presented and compared. The first method is directly linked to the mixed Newtonian-Lagrangian model and it is more accurate, while the second proposed method is based on the strip theory and aims to reconstruct the loads with limited knowledge of the structural model.

To conclude the study, a closed loop control system able to reduce the gust loads is designed. The objective is to decrease fatigue loads and improve passenger comfort by controlling the flexible structure deformations. The control strategy, here proposed, is a Linear Quadratic Regulator (LQR) for the rigid body dynamics, to indirectly reduce the flexible structure response, after a gust, by means of elevator and (symmetric) aileron deflections.

Sommario

L'evoluzione delle strutture aeronautiche e l'uso di materiali sempre più avanzati e leggeri ha portato allo sviluppo di velivoli più efficienti e flessibili. Ciò implica che la sola dinamica del velivolo rigido non è più sufficiente a descriverne il comportamento durante il volo atmosferico. Inoltre, le frequenze dei primi modi propri strutturali si avvicinano a quelle della dinamica del velivolo rigido e pertanto un eventuale accoppiamento tra la dinamica strutturale e le manovre di pilotaggio va considerato durante la modellazione del velivolo. In questa tesi un metodo analitico basato su un approccio misto Newtoniano-Lagrangiano è stato usato per derivare un modello semplificato del velivolo flessibile. Tale modello mantiene un forte legame con le equazioni del moto del velivolo rigido, rendendo l'interpretazione dei termini ottenuti maggiormente intuitiva. Inoltre, gli spostamenti flessibili e le variabili torsionali, entrambi ottenuti mediante le equazioni di Lagrange, vengono fin dall'inizio discretizzati per mezzo del metodo di Galérkin, il quale permette di esprimerli attraverso un numero finito di coordinate generalizzate. Tale approccio permette di derivare direttamente un sistema di ordine finito di equazioni differenziali ordinarie, il che lo rende poco complesso ed adatto per simulazioni in tempo reale e nella definizione delle leggi di controllo. Definito il modello flessibile, un opportuno modello di raffica deve essere utilizzato per valutare la risposta del velivolo. In questo lavoro vengono presentati sia modelli di raffica discreti che continui, entrambi usati per generare grandi carichi alari e per eccitare i modi propri della struttura. Particolare attenzione è stata rivolta a modelli stocastici di turbolenza continua e, pertanto, viene affrontata un'introduzione al concetto di probabilità e ai metodi basati sulle Densità Spettrali di Potenza (PSD). Infine, è stata descritta l'implementazione dei modelli di turbolenza di Dryden e von Kármán, in quanto tra i più utilizzati in fase di design. A questo punto è possibile valutare la risposta del velivolo ad una raffica, sia in termini di deformazione della struttura che di carichi dinamici generati su di essa. In questa tesi vengono presentati due metodi per la ricostruzione dei carichi: il primo è direttamente correlato al modello flessibile qui presentato, mentre il secondo è una semplificazione basata sulla teoria di striscia, il cui obiettivo è quello di ricostruire i carichi supponendo di avere una conoscenza limitata del modello strutturale. Per concludere, viene applicato al modello un sistema di controllo mirato alla riduzione dei carichi di raffica. L'obiettivo è quello di diminuire i carichi a fatica e di migliorare il comfort dei passeggeri andando a controllare la deformazione della struttura flessibile. La strategia di controllo proposta prevede l'utilizzo di un Regolatore Quadratico Lineare (LQR) sulla dinamica del velivolo rigido, in modo di influenzare e ridurre indirettamente la risposta della struttura flessibile ad una raffica attraverso la deflessione dell'equilibratore e degli alettoni.

Contents

List of Figures	3
List of Tables	5
1 Introduction	6
1.1 Thesis Outline	13
2 Aircraft Model	15
2.1 Non-Linear Rigid Model	16
2.2 Aerodynamic Model	17
2.3 Flexible Model	18
2.3.1 Kinetic & Potential Energy	18
2.3.2 Generalized Coordinates: Galérkin Method	21
2.3.3 Generalized Forces	22
2.3.4 Flexible Model Conclusion	26
2.4 Complete Model	26
3 Gust Model	27
3.1 Gust Load Introduction	27
3.2 Discrete Vs. Continuous Gusts	29
3.3 Probability and PSD Concepts	32
3.4 Dryden and von Kármán Turbulence Models	39
4 Wing Response & Load Determination	45
4.1 Wing Response	46
4.2 Load Determination	54
4.2.1 MCK Method	54
4.2.2 Strip Theory	55
4.3 Results Comparison	56

5	Control System Design	61
5.1	State-Space System Definition	62
5.2	Linear Quadratic Regulator (LQR)	65
5.3	Control System Implementation	67
6	Conclusions	71
6.1	Future Developments	73
	Appendices	74
A	Complete Non-Linear Rigid Aircraft Model	75
	Bibliography	79

List of Figures

1.1	Flexible Aircraft Model Presented by Meirovitch and Tuzcu	7
1.2	Typical "1 – cos" Gust Velocity Profiles	9
1.3	Example of Gust Linear Velocity Components - von Kármán	10
1.4	Roesch and Harlan Auxiliary Wing System	11
2.1	Complete Model Scheme	15
2.2	Aircraft Deformations	19
3.1	Example of Vertical Gust	28
3.2	Example of Head-on Gust	29
3.3	Example of Gust Profile	30
3.4	"1 – cos" Discrete Gust Idealization	30
3.5	Example of Gust Sampling	33
3.6	Probability Density	34
3.7	Probability Distribution	34
3.8	$1 - P(y)$ in Logarithmic Scale	35
3.9	Example of Superimposition of Sinusoids	37
3.10	PSD Scheme	37
3.11	Effect of L on PSD	41
3.12	Medium/High Altitude Turbulence Intensities	42
3.13	Continuous Gust Example	44
4.1	Wing Bending Rate after an Elevator Step	48
4.2	Wing Torsion Rate after an Elevator Step	48
4.3	Wing Bending Acceleration after an Elevator Step	49
4.4	Wing Torsion Acceleration after an Elevator Step	49
4.5	"1 – cos" Gust Profile	50
4.6	Wing Bending Acceleration after a "1 – cos" Gust	51
4.7	Wing Torsion Acceleration after a "1 – cos" Gust	51
4.8	Continuous von Kármán Gust Profile	52
4.9	Wing Bending Acceleration after a von Kármán Gust	53

4.10	Wing Torsion Acceleration after a von Kármán Gust	53
4.11	Distributed Loads Over The Wing Span	55
4.12	Wing Root Bending Moment - Deformation Only - Step of δ_e	57
4.13	Wing Root Torsion Moment - Deformation Only - Step of δ_e	57
4.14	Wing Root Bending Moment - Deformation Only - "1 - cos"	58
4.15	Wing Root Torsion Moment - Deformation Only - "1 - cos"	58
4.16	Wing Root Bending Moment - Deformation Only - von Kármán	59
4.17	Wing Root Torsion Moment - Deformation Only - von Kármán	59
5.1	Closed Loop System Scheme	66
5.2	Open Loop Vs. Closed Loop Eigenvalues	67
5.3	Open Loop Vs. Closed Loop - Bending Moment - "1 - cos" Discrete Gust	68
5.4	Open Loop Vs. Closed Loop - Torsion Moment - "1 - cos" Discrete Gust	69
5.5	Open Loop Vs. Closed Loop - Bending Moment - von Kármán Gust	69
5.6	Open Loop Vs. Closed Loop - Torsion Moment - von Kármán Gust	70
A.1	Body Axes Reference Frame	76

List of Tables

4.1	General Aircraft Data	46
5.1	LQR Controller Data	68

Chapter 1

Introduction

The progress in aerospace materials has led to the creation of more light and slender aircraft structures. This results in both weight and drag reduction, and consequently in more efficient aircraft in terms of fuel consumption. On the other hand, this slender structures tend to be highly deformable, and thus the assumption of rigid body used in classical flight mechanics is no longer a valuable option when modelling the aircraft. The deformation of the structure increases fatigue loads by means of the the dynamic loads generated by the aircraft manoeuvres or by external perturbations. Also more flexibility leads to lower frequencies of the structural modes which might couple with typical aircraft dynamics frequencies [1] resulting in dangerous resonance phenomena.

For these reasons is necessary to define a complete model which takes in account of the flexible dynamics of the aircraft structure. Such models have been a subject of study not only in recent years, but comprehensive mathematical formulations of the problem have been derived for both structural dynamics [2] and aeroelastic [3] purposes. The problem of the majority of these formulations is that are not suitable for real-time applications because of their high complexity level. Therefore, a good compromise between model accuracy and computational cost must be found.

First flexible aircraft models have been studied starting from the early 1960s. At that time strong simplifications were needed in order to obtain a solution of the equations, because of the lack of computational power. One of the most important works of that period was presented by Milne [4] in 1964. This study consisted of developing a model considering only the longitudinal motion of the aircraft under the assumption of both small deformations and state variable variations. Particular attention was given to the choice of the best set of axes between attached, mean and principle axes. The final result led to the mean axes as the best choice, since in this set of axes the deformation rate does not affect the angular momentum, permitting to decouple rigid and flexible degrees of freedom.

From this starting point, the development of flexible models has taken different

directions. In 1977 Cavin and Dusto [5] presented a model based on Hamilton's principle, in which approximate results were obtained by means of finite-elements method. Then, in 1987 Butril, Zeiler and Arbuckle [6] presented an integrated non-linear flexible model of the F/A-18 aircraft using the Lagrange's equations in a mean axes reference frame. The problem in this approach is that the mean axes position it is difficult to determine, affecting the model accuracy and requiring adequate measurements on-board the aircraft.

Years later, specifically in 2004, Meirovitch and Tuzcu [7] presented a model based on Lagrange's equations but without the need to determine the mean axes position. Their approach consists in deriving an hybrid system of ordinary and partial differential equations in terms of quasi-coordinates (or generalized coordinates), which permits to express the transport degrees of freedom in terms of flight variables, as linear and angular velocities. This is convenient for real time simulation of the flexible structure but compromises the simplicity of the formulation, since the Lagrange's equation has to take in consideration additional terms and, also, the obtained hybrid system of ordinary and partial equations needs some form of discretization.

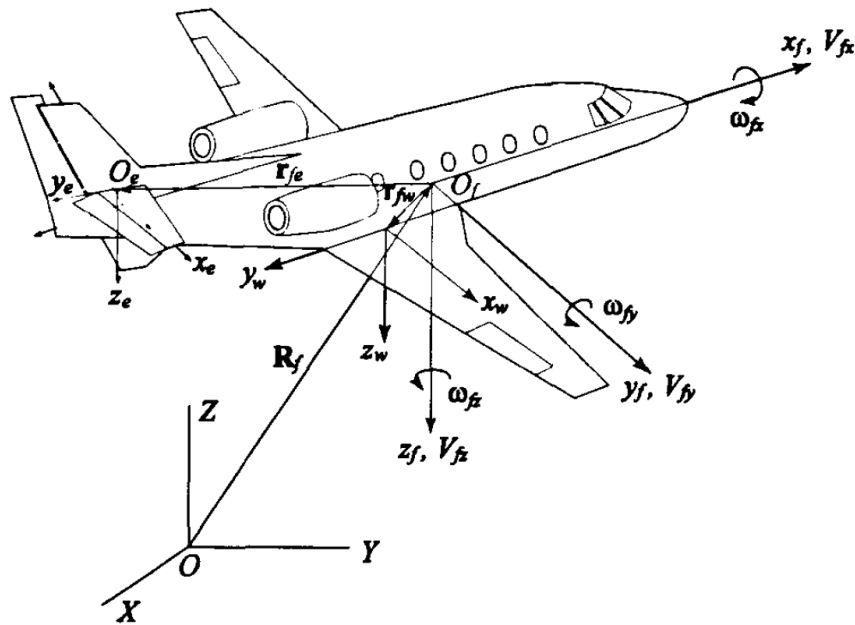


Figure 1.1: Flexible Aircraft Model Presented by Meirovitch and Tuzcu

The model presented in this thesis takes as main reference the work of Avanzini, Capello and Piacenza [8], which is based on the aforementioned Meirovitch and Tuzcu article. Their objective was to derive a minimum-complexity flexible model

which takes in account the effects of bending and torsion of fuselage and wings on the aircraft rigid dynamics. This is done by means of a mixed Newtonian-Lagrangian approach, using the classical equations of flight dynamics to derive the rigid degrees of freedom and the Lagrange's equations to derive the flexible terms. Splitting the problem in these two parts and expressing from the beginning the deformation variables in terms of quasi-coordinates, not only simplifies the interpretation of the terms but also permits to write directly a system of ordinary differential equations, without passing through the hybrid system derived by Meirovitch and Tuzcu. This approach, although introduces some simplifications, is particularly convenient for real time simulation and for the design of control laws which take in consideration the flexible body interaction with the aircraft flight dynamics. Furthermore, this model represents a good foundation for studying the response and the loads of the flexible parts, not only during the aircraft manoeuvres but also to external gusts.

For this reason, in this thesis particular attention is given to the gust modelling and its implementation in the presented model. Regulations as CS-25 [9] require to simulate different gusts during the aircraft design phase, in order to identify the loads generated by these perturbations and, thus, verify that the flight envelope limits are not exceeded. Gust models are generally divided in:

- **Discrete** gusts: The gust is idealized as a single finite disturb with a specific "shape".
- **Continuous** gusts: The gust is idealized as a series of concatenated disturbs of varying intensity. In general these gusts are generated as stochastic processes.

One of the must used discrete gust models, which is also reported in both in military and civil regulations, is the "1 – cos" gust idealization. This gust shape is widely used since permits to simulate a wide range of perturbations, as reported in Figure 1.2, by means of two parameters: H and U_{ds} . The first is called gust gradient and identifies if the perturbation is small or large and, thus, if it is rapid or slow. The gust design velocity U_{ds} , instead, identifies the perturbation intensity by defining the maximum reachable peak in terms of gust speed. Both of this parameters have to be scaled accordingly with the flight altitude and with the aircraft mass configuration. Regulations require that a wide set of perturbations is tested during aircraft design, in the entire altitude range indicated by the flight envelope.

This gust idealization is particularly convenient for the ease with which can be applied, and in general is used to simulate large loads on the entire aircraft. Anyway, it is not an accurate representation of the random nature of the atmospheric turbulences. Especially if the objective is to excite the various elastic modes of the flexible structure. In this case it is necessary to implement continuous gust models in order to study the effect of a more realistic turbulence on the flexible structure.

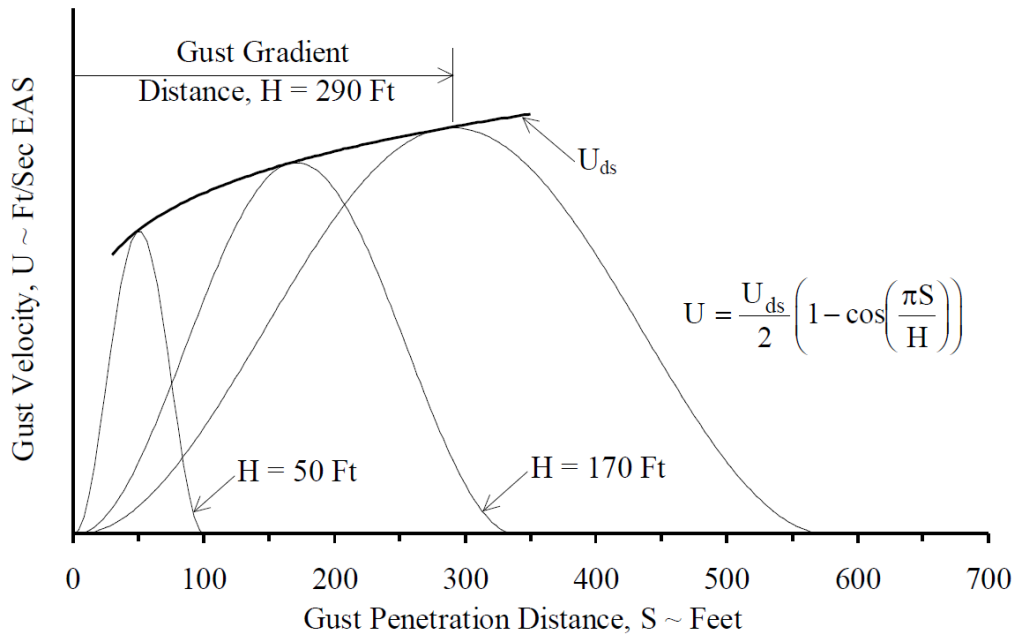


Figure 1.2: Typical "1 - cos" Gust Velocity Profiles

Continuous gust models express the turbulence as a stochastic process which varies randomly in space and time. In practice, to describe mathematically the turbulence, the gust is generally idealized as a "stationary Gaussian random process" [10], which, although is a simplification, leads to more realistic results than the discrete gust models. The two most used continuous gust models, are the Dryden [11] and von Kármán [12] turbulence models. Both define the gust by means of mathematical expressions of the Power Spectral Densities (PSD) of the various velocity components. These Power Spectral Densities can be then used to design "forming filters" which take as input a white noise and output a gust time history based on Dryden and von Kármán models. The Dryden model has rational PSD for every velocity component and, thus, an exact filter can be designed. The von Kármán, instead, has irrational PSDs and thus the forming filters can be only approximated. Also, the von Kármán model results to be the more accurate between the two models and, in fact, it is the only one which is implemented in both military [13] and civil [9] regulations.

In practice both Dryden and von Kármán models give as output the gust linear and angular velocities components time histories, as in the example in Figure 1.3, which can be used in the rigid aircraft equations of motions as wind disturbances. In this way the entire model is affected by the external perturbations and thus the flexible structure response can also be analysed.

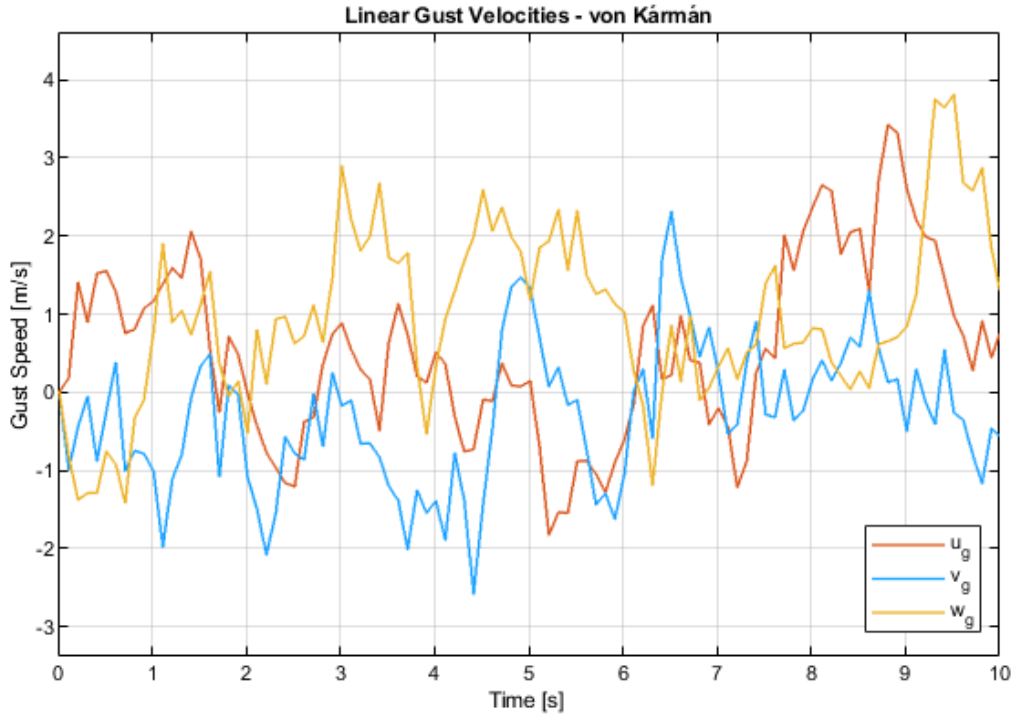


Figure 1.3: Example of Gust Linear Velocity Components - von Kármán

As stated before, this flexible structure response not only affects the aircraft rigid dynamics but also generates dynamic loads which are directly connected to the deformations and their respective rates. These loads can be determined starting from the flexible model or by approximating the loads depending only on the variation of the local angle of attack. The first method is surely more accurate, but requires the definition of a flexible model and, thus, some structural data obtained, generally, with a prior FEM analysis. On the other hand, the second method can be applied knowing only the deformations and their respective rates, which can be also measured with sensors on the surface, but neglecting some structural information.

In any case, since the objective is not to calculate the fatigue strength of the components, but to evaluate the effectiveness of a controller designed for gust load alleviation (GLA) purposes, the approximations introduced by both the previously mentioned methods can be considered acceptable.

Alleviation of the dynamic loads generated by gusts is subject of study since the 1950s [14], but only in recent years, with the more extended use of composite materials, the interest in this type of systems is renewed.

Gust load alleviation systems, in general, can be divided in two macro categories, which differentiate for the type of control action:

- **Passive** systems: do not require an actuation system and in general are related to the wing geometry.
- **Active** systems: require an actuation system and rely on the regular control surfaces, as ailerons and elevators, or on unconventional control surfaces designed for the purpose of load alleviation. In general, a specifically designed control law is needed.

One interesting passive gust alleviation system concept was presented by Roesch and Harlan [15] in 1974. The main topic of the study was to develop a gust load alleviation method which was suitable for small aircraft, and thus not requiring the installation of a heavy actuation system. They observed that a good wing load alleviation could be obtained by means of trailing edge flaps, and imagined that those surfaces could be directly actuated by two small auxiliary wings, as in Figure 1.4. These wings were, in practice, an angle of attack sensor large enough to drive the flaps directly. Therefore, these devices were articulated in roll to deflect the flaps and in pitch for coupling to the elevator and maintaining basic manoeuvrability, since this device induced stability issues. Although their method can not be applied on large aircraft, two important concepts can be extracted from Roesch and Harlan study: the load dependence on the angle of attack and the necessity of specifically designed control surfaces on the wing.

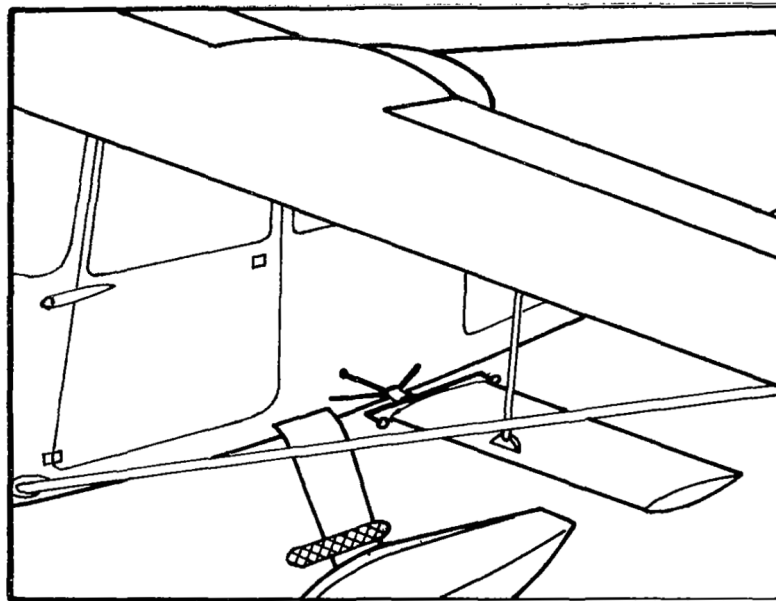


Figure 1.4: Roesch and Harlan Auxiliary Wing System

More recent studies, thanks also to the CFD development, demonstrate that passive gust load alleviation can be achieved by passive twist of the wing-tip, as

in [16], or, even more recently, by means of passive ventilation with porous surface and deflectable vanes [17]. In general, passive methods are more simple and reliable of the active methods, since they do not require power or any interaction with the aircraft systems. On the other hand, they can not deal with more severe turbulences and can not provide load control if it is needed.

For these reasons, active gust load alleviation systems are, at the moment, the most studied and implemented during the aircraft design. These systems differentiate mostly for the control surface used for the alleviation, generally conventional and unconventional, and for the chosen controller architecture.

One possible approach, consist in to controlling directly the flexible part by means, for example, of symmetric deflection of the ailerons. This can be done by means of an adaptive feedforward controller as presented Zeng et al. in [18]. The approach presented in their paper consisted in the design of a FIR (Finite Impulse Response) filter based on the LMS (Least Mean Square) algorithm [19]. In practice the goal of this filter its to reduce an error between a selected reference signal and a desired signal. For example, in Zeng work, the flexible acceleration of the wing is compared with the rigid acceleration of the center of mass, then the generated error is reduced via LMS algorithm. This approach, although is very effective, brings some complications. The first consist in to selecting significant reference and desired signal, especially if the equations of aircraft and flexible dynamics are in a dimensional form. In fact, since the output of the filter is a command, and the input signal is an acceleration, there is no mean to scale the output properly. Therefore, this approach requires the knowledge of a state-space formulation of the complete model, which is not always practical to determine, for both the non-linear nature of the system and for the complexity of determining the complete state vector.

Another approach consist in to apply a linear optimal control technique to the aircraft plant as presented by Dillsaver in [20]. This is done by means of an LQR [21] (Linear Quadratic Regulator) controller which is used to determine an optimal state feedback gain. This controller its also used in dual loop configurations, as presented by Gonzalez in [22]: one inner loop for augmenting the aircraft stability and minimizing elastic displacements and an outer loop for altitude, heading and speed control.

Other widely spread control design techniques used for gust load alleviation purposes are represented by the implementation of \mathcal{H}_2 and \mathcal{H}_∞ robust controllers, as proposed by Aouf, Boulet and Botez in [23]. Their work consisted on implementing an \mathcal{H}_∞ controller on a flexible model of the B-52 aircraft, achieving a strong gust load alleviation for severe turbulences simulated with the Dryden model. However, from their work emerged that the result consistency is strongly dependant on the considered aircraft model. This was also demonstrated by Cook et al. in [24], which have combined robust control with model-reduction methodologies. While they

obtained a load reduction up to 9% on root bending moment, they also highlighted a significant decrease in control performance if even small uncertainties were added to the model.

A more comprehensive gust load alleviation technique is given by the \mathcal{L}_1 adaptive controller developed by Capello et al. in [25]. The advantage of this controller consists in its capacity to adapt to the uncertainties deriving from the weight and flight condition variation. With this approach, the author was able to obtain an average 20% wing load reduction between different mass and flight condition configurations.

In this thesis, since the proposed aircraft model maintains a strong link between rigid aircraft dynamics and the flexible dynamics, a LQR controller is implemented. One of the major difficulties of the presented problem, as already stated before, is to write the entire system in a state-space form. The advantage of the presented model is the possibility to implement an LQR controller only on the rigid equation of motion, and thus indirectly influencing the flexible model. This is a more straightforward method, since the state-space model formulation of the aircraft rigid dynamics is already well known. The LQR controller acts on the rigid states influenced by the external perturbation and outputs elevators and symmetric ailerons commands. Then the controlled states are used in the flexible dynamics model, and the resulting loads are compared with the open loop response.

1.1 Thesis Outline

After this brief introduction, Chapter 2 contains the derivation of the complete model, starting from the longitudinal non-linear rigid equations of motion and a brief description of the aerodynamic model. Then the flexible dynamics model of the wing is derived by means of the Lagrangian approach. Finally, the section at the end of the chapter briefly describes how to use the obtained flexible displacements (and rates) to correct the aircraft rigid equations of motion.

Chapter 3 is focused on the description of the gust models used to perturb the aircraft. After an introduction to the gust loads, a comparison between discrete and continuous gust models is addressed. Then, in order to better describe the latter, some basic concepts of probability and Power Spectral Density (PSD) theory are given. The last section is dedicated to the description of the Dryden and von Kármán continuous turbulence models and how these are implemented in the simulations.

In Chapter 4 are reported the results in terms of wing response and dynamic loads. The wing response is evaluated in terms of bending and torsion rates and accelerations achieved after an elevator step command, a "1 – cos" discrete gust and von Kármán moderate turbulence. Then, two different methods for the determination of the dynamic loads are described: one based on the MCK definition of the flexible system and one based on the strip theory. Finally, the results in terms of root

bending and torsion moments obtained with both the load determination methods are compared, analysing their accuracy for both the discrete and continuous gusts mentioned above.

Chapter 5 is dedicated to the design and implementation of the proposed gust load alleviation control strategy. The first part of the chapter is dedicated to the derivation of the non-dimensional state-space formulation of the system. Then the design of the LQR controller is addressed, describing the algorithm and reporting the chosen gain matrices. The last part of the chapter is dedicated to the comparison between open loop and closed loop results, in terms of root bending and torsion moments reduction for both the "1-cos" discrete gust and the von Kármán moderate turbulence.

Finally, in Chapter 6 are contained some concluding remarks and some possible future developments of this work.

Chapter 2

Aircraft Model

The complete aircraft model can be seen as an interaction between three major blocks:

- Rigid aircraft model
- Aerodynamic model
- Flexible model

Particularly, the latter acts as a correction to the first two, adding the displacements due to elastic deformation to the rigid model and the aerodynamic loads which this deformation generates to the aerodynamic model, as schematized in Figure 2.1.

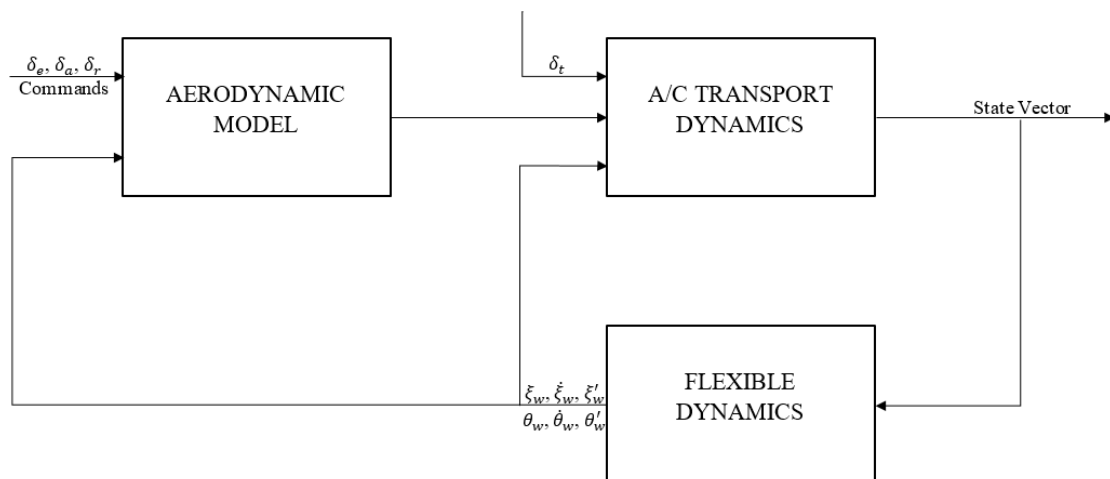


Figure 2.1: Complete Model Scheme

In this work particular attention is given to the flexible model, since the objective is to study the wing load behavior under a gust disturbance. However, wing deformation is caused by both aerodynamic and inertial loads, which can be evaluated only considering the rigid aircraft dynamics and an appropriate aerodynamic model. For this reason and for the sake of completeness, in this chapter each part of the model will be briefly discussed, including also how to correct the rigid model with flexible dynamics.

2.1 Non-Linear Rigid Model

The rigid model is based on the non-linear dimensional equations of motion written in the body axes frame as reported in [26]. The resulting 6 DoF differential equation system takes in consideration 12 variables, that are:

- Linear velocities $\{u, v, w\}$, from force equations.
- Angular rates $\{p, q, r\}$, from moment equations.
- Euler angles $\{\phi, \theta, \psi\}$, from kinematic equations.
- Coordinates $\{x_N, y_E, z_D\}$, from navigation equations (NED¹ reference frame).

Derivation of the complete rigid model is given in Appendix A. Here, for simplicity, since only the longitudinal dynamics components are taken in consideration in the flexible model, the entire system could be reduced neglecting the lateral-directional equations components, thus obtaining:

$$\begin{cases} \dot{u} + qw = \frac{1}{m}(X + T_{max}\delta_T) - g \sin \theta \\ \dot{w} + uq = \frac{1}{m}Z + g \cos \theta \\ \dot{q} = \frac{1}{I_y}M \\ \dot{\theta} = q \end{cases} \quad (2.1)$$

Where earth rotation and round earth corrections are considered already applied. Also the effect of throttle δ_T is taken in consideration. The aerodynamic forces and

¹North-East-Down

moments X , Z and M can be written as:

$$X = \frac{1}{2}\rho V^2 S C_X \quad (2.2)$$

$$Z = \frac{1}{2}\rho V^2 S C_Z \quad (2.3)$$

$$M = \frac{1}{2}\rho V^2 S c C_M \quad (2.4)$$

In which the aerodynamic coefficients C_X , C_Z and C_M are function of the angle of attack α , the non-dimensional pitch rate $\bar{q} = \frac{q\bar{c}}{V}$ and the commands, that is δ_e if the only longitudinal dynamics are considered.

$$C_i = C_i(\alpha, \bar{q}, \delta_e) \quad \text{with } i = X, Z, M \quad (2.5)$$

Finally the angle of attack α and the airspeed V are proper of the wind axes, therefore they need to be expressed in body axes:

$$\alpha = \tan \frac{w}{u} \quad (2.6)$$

$$V = \sqrt{u^2 + w^2} \quad (2.7)$$

2.2 Aerodynamic Model

For a correct interaction between the various blocks of the complete model, aerodynamic modelization of the wing should express the loads in the same reference frame of the rigid and flexible models. Furthermore, for the purpose of this work, it is important to find a good balance between load estimation accuracy and model complexity, which would translate in a computational load increase.

For this reason, the strip theory, as described in [3], was selected for the aerodynamic load estimation. The 3D effects associated with finite elongation wings (e.g. tip vortices) are neglected, preferring a 2D analysis. The wing is thus divided into sections along the wing span and each of them has its own resistance, lift and aerodynamic moment. Lift of each section is then considered to depend only on the local incidence given by the 2D theory and to be independent from the angle of attack of any other section. The total lift is therefore obtained by integrating the aerodynamic load of each station along the wing span.

Drag coefficient of each section can be evaluated by the following quadratic relation:

$$C_D = C_{D0} + kC_L^2 \quad (2.8)$$

This approach permits to easily determine the aerodynamic loads of each section by simply knowing its angle of attack variation, which could be due either from a maneuver or a gust disturbance and the resulting wing deformation.

2.3 Flexible Model

The chosen method to describe the flexible aircraft dynamics is based on the mixed Newtonian-Lagrangian approach, which is largely discussed in [7] and [8]. In this work only the wings are considered to be deformable while the rest of the aircraft is considered to be rigid, although the reference method could also consider the fuselage and the tail as deformable.

In the general form, Lagrange's equations can be written as:

$$\frac{d}{dt} \frac{\partial \mathcal{L}}{\partial \dot{q}} - \frac{\partial \mathcal{L}}{\partial q} = Q_q \quad (2.9)$$

Where q represents the generalized coordinates, Q_q represents the generalized forces and \mathcal{L} is the Lagrangian, defined as:

$$\mathcal{L}_{(t)} = \mathcal{T}_{(t)} - \mathcal{U}_{(t)} \quad (2.10)$$

With \mathcal{T} and \mathcal{U} respectively kinetic and potential energy. Once every component of the Lagrange's equation is calculated, it will be possible to determine the elastic deformation of the wing, that can be also used to correct the rigid model dynamics. The scheme in Figure 2.2 shows how elastic deformations affect the entire aircraft, including fuselage and tail which in this thesis, as already stated before, are considered rigid.

2.3.1 Kinetic & Potential Energy

The kinetic energy of the entire system is given by the sum of the kinetic energy of each system component. In this thesis, the aircraft is considered to be divided in rigid fuselage and flexible wings, thus obtaining:

$$\mathcal{T}_{(t)} = \mathcal{T}_{RIG(t)} + 2\mathcal{T}_{w(t)} \quad (2.11)$$

Where, from here on, the subscript RIG indicates the rigid fuselage and the subscript w indicates the flexible wing. In general:

$$\mathcal{T}_{RIG} = \frac{1}{2} m_{RIG} (V_{RIG} \cdot V_{RIG}) + \frac{1}{2} \Omega_{RIG}^T J_{RIG} \Omega_{RIG} \quad (2.12)$$

$$\mathcal{T}_w = \frac{1}{2} \int_0^{l_w} \mu_w \dot{R}_w \cdot \dot{R}_w dx_w + \frac{1}{2} \int_0^{l_w} \Omega_w^T j_w \Omega_w dx_w \quad (2.13)$$

Where Ω_{RIG} and V_{RIG} are respectively the angular rate vector and the linear velocity vector of the rigid fuselage, μ_w represents the mass density per unit of length and j_w is the inertial tensor of the wing element. Finally, \dot{R}_w and Ω_w are respectively the

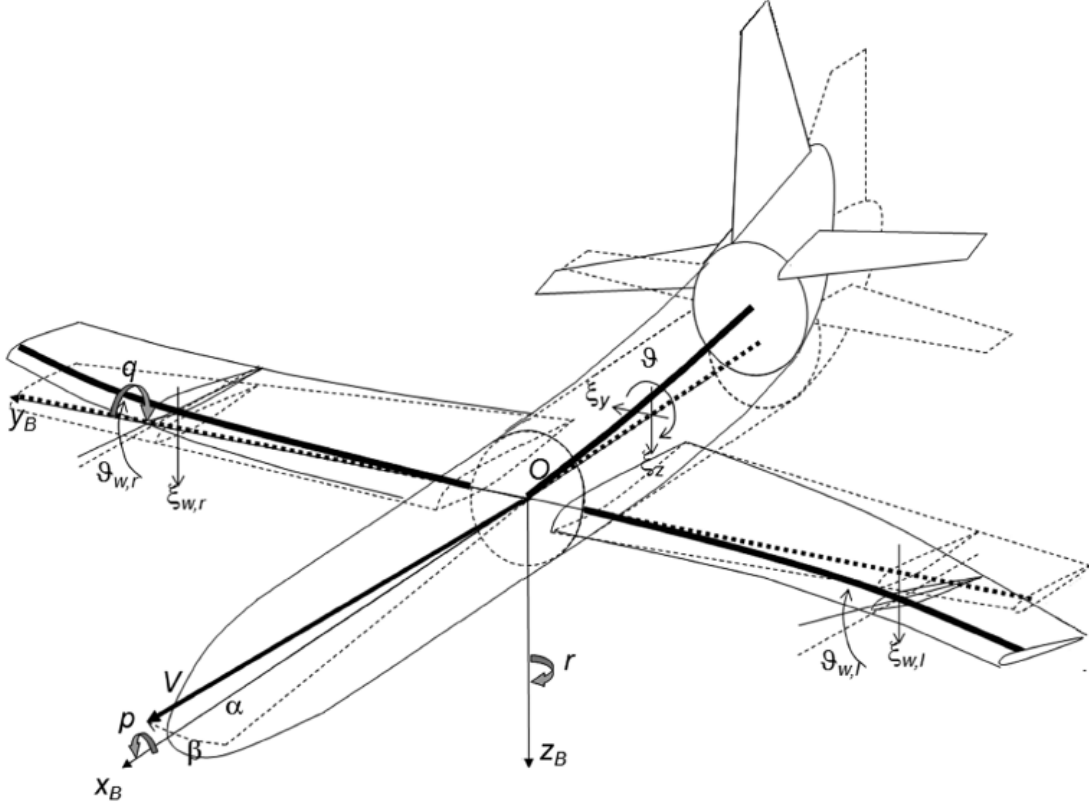


Figure 2.2: Aircraft Deformations

linear velocity vector and the angular rate vector which take into account of wing deflection ξ_w and torsion θ_w . In general, those are expressed as:

$$\dot{R}_w = V_B + \omega_B \times r_w + \dot{\xi}_w \quad (2.14)$$

$$\Omega_w = \omega_B + \dot{\theta}_w \times \hat{t}_w + \dot{\xi}'_w \quad (2.15)$$

Where V_B and ω_B are linear and angular speed vectors in body reference frame, r_w is the position of the considered wing element in the wing reference frame and \hat{t}_w is the torsion axis. Symbols $(\dot{\quad})$ and $(\quad)'$ represent respectively time and space derivative. In this case Eq. 2.14 and 2.15 become:

$$\dot{R}_w = \begin{Bmatrix} u \\ v \\ w \end{Bmatrix} + \begin{Bmatrix} p \\ q \\ r \end{Bmatrix} \times [C_w]^T \begin{Bmatrix} x_w \\ y_w \\ z_w + \xi_w \end{Bmatrix} + [C_w]^T \begin{Bmatrix} 0 \\ 0 \\ \dot{\xi}_w \end{Bmatrix} \quad (2.16)$$

$$\Omega_w = \begin{Bmatrix} p \\ q \\ r \end{Bmatrix} + [C_w]^T \begin{Bmatrix} \dot{\theta}_w \\ 0 \\ 0 \end{Bmatrix} + \begin{Bmatrix} 0 \\ -\dot{\xi}'_w \\ 0 \end{Bmatrix} \quad (2.17)$$

Where $[C_w]$ is a rotational matrix used to transport a vector from the body reference frame to a wing reference frame, taking in account the sweep angle Λ and the dihedral angle Γ of the wing. In this thesis, as in [8], the wing reference frame has the x_w axis along the wingspan, z_w axis that points downwards and the y_w axis that completes the frame following the right-handed rule. Considering this wing reference frame positioning, $[C_w]$ should be expressed as:

$$C_w = \begin{bmatrix} -\sin \Lambda \cos \Gamma & \cos \Lambda \cos \Gamma & -\sin \Gamma \\ -\cos \Lambda & -\sin \Lambda & 0 \\ -\sin \Lambda \sin \Gamma & \cos \Lambda \sin \Gamma & \cos \Gamma \end{bmatrix} \quad (2.18)$$

Although, for simplicity, dihedral and sweep angles are considered to be null in this work, $[C_w]^T$ is used in Eq. 2.16 and 2.3.1 to express all elements in body reference frame. Knowing this, and expressing the cross product in Eq. 2.16 in matrix form by means of the skew-symmetric matrix:

$$[\omega_B \times] = \begin{bmatrix} 0 & -r & q \\ r & 0 & -p \\ -q & p & 0 \end{bmatrix} \quad (2.19)$$

Expressions of \dot{R}_w and Ω_w become:

$$\dot{R}_w = \begin{Bmatrix} u \\ v \\ w \end{Bmatrix} + \begin{Bmatrix} -rx_w + q(z_w + \xi_w) \\ -ry_w - p(z_w + \xi_w) \\ px_w + qy_w \end{Bmatrix} + \begin{Bmatrix} 0 \\ 0 \\ \dot{\xi}_w \end{Bmatrix} \quad (2.20)$$

$$\Omega_w = \begin{Bmatrix} p \\ q \\ r \end{Bmatrix} + \begin{Bmatrix} 0 \\ \dot{\theta}_w \\ 0 \end{Bmatrix} + \begin{Bmatrix} 0 \\ -\dot{\xi}'_w \\ 0 \end{Bmatrix} \quad (2.21)$$

Where distances x_w , y_w and z_w now must also take in account the distance between the aircraft CG and the origin of the wing reference frame. Note that, although structural flexibility terms could be small, they cannot be neglected as it is impossible to know in advance the entity of the rigid ones.

The potential energy can be written as the sum of the elastic energy of the system flexible parts plus gravitational potential. In this work, since the wing is the only flexible part, the potential energy can be written as:

$$\mathcal{U} = \mathcal{U}_{wb} + \mathcal{U}_{wt} + \mathcal{U}_{wg} \quad (2.22)$$

Where \mathcal{U}_{wb} is the potential energy due to the wing bending, which can be expressed as strain energy of an Euler-Bernoulli beam:

$$\mathcal{U}_{wb} = \frac{1}{2} \int_0^{l_w} EI_w (\xi_w'')^2 dx_w \quad (2.23)$$

In a similar fashion, the potential energy due to the wing torsion \mathcal{U}_{wt} can be written as:

$$\mathcal{U}_{wt} = \frac{1}{2} \int_0^{l_w} E J_{t,w} (\theta'_w)^2 dx_w \quad (2.24)$$

At last, the potential energy due to the change in altitude caused by the wing bending \mathcal{U}_{wg} , considering dihedral angle to be null, can be expressed as:

$$\mathcal{U}_{wg} = \int_0^{l_w} \mu_w g (\xi_w \cos \theta) dx_w \quad (2.25)$$

Note that, in the above equations only the half-wing is considered, therefore the potential energy components must multiplied by 2 in order to consider the entire wing.

2.3.2 Generalized Coordinates: Galérkin Method

In order to represent the behavior of a flexible system, reducing the model complexity, an appropriate set of generalized coordinates must be chosen. The Galérkin method [27], permits to represent the wing deformation over time through truncated series expansions in the form:

$$\xi_w(x_w, t) = \sum_{j=1}^N \Phi_j(x_w) \eta_j^w(t) \quad (2.26)$$

$$\theta_w(x_w, t) = \sum_{j=1}^N \Psi_j(x_w) \zeta_j^w(t) \quad (2.27)$$

Where $\eta_j^w(t)$ and $\zeta_j^w(t)$ are amplitudes of the assumed modes represented by $\Phi_j(x_w)$ and $\Psi_j(x_w)$ shape functions, which should satisfy the physical and geometric boundary conditions of the considered element. For example, for a generic cantilevered beam:

$$\Phi_i(x) = \cosh\left(\frac{\lambda_i}{l}x\right) - \cos\left(\frac{\lambda_i}{l}x\right) + \chi_i \left(\sinh\left(\frac{\lambda_i}{l}x\right) - \sin\left(\frac{\lambda_i}{l}x\right) \right) \quad (2.28)$$

Where:

$$\chi_i = \frac{\cosh\left(\frac{\lambda_i}{l}\right) + \cos\left(\frac{\lambda_i}{l}\right)}{\sinh\left(\frac{\lambda_i}{l}\right) + \sin\left(\frac{\lambda_i}{l}\right)} \quad (2.29)$$

and l is the beam length and λ_i is the eigenvalue solution of:

$$\cos \lambda_i \cosh \lambda_i = -1 \quad (2.30)$$

The choice of shape functions and generalized coordinates number N , influences the number of vibrational modes considered. In this case only the first two bending modes and the first torsional mode were considered, since these have frequencies similar to the ones representing the rigid aircraft dynamics:

$$\xi_w(x_w, t) = \Phi_1(x_w)\eta_1^w(t) + \Phi_2(x_w)\eta_2^w(t) \quad (2.31)$$

$$\theta_w(x_w, t) = \Psi_1(x_w)\zeta_1^w(t) \quad (2.32)$$

Once the set of generalized coordinates is selected, it is possible to obtain and derive the expressions of kinetic and potential energy, thus obtaining the left side of the Lagrange's equation. Note that the obtained derivatives have the same form for each generalized coordinate, independently from the number of flexible modes considered.

2.3.3 Generalized Forces

In order to complete the Lagrange's equation also the generalized forces Q_q must be obtained. These can be derived through the principle of virtual work, which for the dependant variable r in presence of k external forces can be expressed as:

$$\partial W = \sum_{h=1}^k F_h \cdot \partial r_h \quad (2.33)$$

where ∂r is the virtual displacement which could be also expressed in terms of the N generalized coordinates:

$$\partial r_h = \sum_{j=1}^N \frac{\partial r_h}{\partial q_j} \partial q_j \quad (2.34)$$

thus obtaining:

$$\partial W = \sum_{h=1}^k F_h \sum_{j=1}^N \frac{\partial r_h}{\partial q_j} \partial q_j = \sum_{j=1}^N \left(\sum_{h=1}^k F_h \frac{\partial r_h}{\partial q_j} \right) \partial q_j = \sum_{j=1}^N Q_{q_j} \partial q_j \quad (2.35)$$

Therefore, in Eq. 2.35 the virtual work is expressed as function of generalized coordinates and forces, which are expressed as:

$$Q_{q_j} = \sum_{h=1}^k F_h \frac{\partial r_h}{\partial q_j} \quad \text{with } j = 1, \dots, N \quad (2.36)$$

In this study, the virtual work of each flexible part can be expressed as a function of external forces that act on it (i.e., aerodynamic distributed and concentrated

loads) multiplied by the virtual displacements, which are the dependent variables. So, similarly to Eq. 2.33, for the flexible wing is possible to write:

$$\partial W_{w,b} = \int_0^{l_w} f_{Aw}(\alpha_w, x_w) \xi_w(x_w, t) dx_w \quad (2.37)$$

$$\partial W_{w,t} = \int_0^{l_w} M_{Aw}(\alpha_w, x_w) \theta_w(x_w, t) dx_w \quad (2.38)$$

where f_{Aw} and M_{Aw} represent the distributed aerodynamic force and moment generated by the wing. Note that, if the aircraft engine is mounted under the wing, a concentrated load must be considered at the corresponding wing section. As stated in section 2.2, in this thesis the aerodynamic loads of each section are considered to be dependant only on the angle of attack and its variation due the maneuver and wing deformation. Therefore, aerodynamic force and moment can be expressed, for the entire wing, as:

$$f_{Aw} = \frac{1}{2} \rho V^2 S C_{L\alpha} \alpha_w \quad (2.39)$$

$$M_{Aw} = \frac{1}{2} \rho V^2 S C_{L\alpha} (x_\theta - x_{CA}) \alpha_w \quad (2.40)$$

where $(x_\theta - x_{CA})$ represents the distance between the torsion axis and the airfoil aerodynamic center, and α_w is given by the sum of aircraft angle of attack α_{WB} , wing twist angle i_w , pitch rate q , bending rate $\dot{\xi}$, torsion angle θ and its time derivative $\dot{\theta}$:

$$\alpha_w = \alpha_{WB} + i_w(x_w) - \frac{qx_F}{u} + \frac{\dot{\xi}_w}{u} + \theta_w + \frac{\dot{\theta}_w(x_\theta - x_{CA})}{u} \quad (2.41)$$

Where x_F represents the distance between the aerodynamic centre of the considered section and the aircraft CG in body reference frame.

More accurately, external aerodynamic force and moment can be written in the form:

$$f_{Aw}(x) = f_{A_0} + \frac{\partial f_A}{\partial \dot{\xi}_w} \dot{\xi}_w \quad (2.42)$$

$$M_{Aw}(x) = M_{A_0} + \frac{\partial M_A}{\partial \dot{\theta}_w} \dot{\theta}_w \quad (2.43)$$

where the subscript 0 indicates the aerodynamic load generated by the “frozen” configuration, for the current values of transport and deformation variables, whereas the second term indicates the increment generated by deformation rates. This approach permits to split the virtual work, expressed for the k -th wing element, in two contributions:

$$\partial W_{k,b} = \int_0^{l_k} f_A \delta \xi dx_k = \int_0^{l_k} f_{A_0} \delta \xi dx_k + \int_0^{l_k} \left(\frac{\partial f_A}{\partial \dot{\xi}} \dot{\xi} \right) \delta \xi dx_k \quad (2.44)$$

$$\partial W_{k,t} = \int_0^{l_k} M_A \delta \theta dx_k = \int_0^{l_k} M_{A_0} \delta \theta dx_k + \int_0^{l_k} \left(\frac{\partial M_A}{\partial \dot{\theta}} \dot{\theta} \right) \delta \theta dx_k \quad (2.45)$$

The contribution to the virtual work of the "frozen" term generated by aerodynamic force and moment can be simply expressed as:

$$\begin{aligned} \int_0^{l_k} f_{A_0} \delta \xi dx_k &= \\ &= \int_0^{l_k} \frac{1}{2} \rho V^2 S c^{(k)} C_{L\alpha} \left[\alpha_{WB} + \theta_{w,k} - \frac{q}{u} x_F \right] \left(\Phi_1^{(k)} \delta \eta_1 + \Phi_2^{(k)} \delta \eta_2 \right) dx_k \end{aligned} \quad (2.46)$$

$$\begin{aligned} \int_0^{l_k} M_{A_0} \delta \theta dx_k &= \\ &= \int_0^{l_k} \frac{1}{2} \rho V^2 S c^{(k)} C_{L\alpha} (x_\theta - x_{CA}) \left[\alpha_{WB} + \theta_{w,k} - \frac{q}{u} x_F \right] \left(\Psi_1^{(k)} \delta \zeta_1 \right) dx_k \end{aligned} \quad (2.47)$$

In which $c^{(k)}$ is the chord of the k -th wing element.

The second term of Eq. 2.44 and 2.45, generated by deformation rates, can be expressed in terms of Rayleigh dissipation function \mathcal{F} [2]:

$$\int_0^{l_k} \left(\frac{\partial f_A}{\partial \dot{\xi}} \dot{\xi} \right) \delta \xi dx_k = \sum_{j=1}^N \frac{\partial \mathcal{F}_b^{(k)}}{\partial \dot{\eta}_j} \delta \eta_j = \frac{\partial \mathcal{F}_b^{(k)}}{\partial \dot{\eta}_1} \delta \eta_1 + \frac{\partial \mathcal{F}_b^{(k)}}{\partial \dot{\eta}_2} \delta \eta_2 \quad (2.48)$$

$$\int_0^{l_k} \left(\frac{\partial M_A}{\partial \dot{\theta}} \dot{\theta} \right) \delta \theta dx_k = \sum_{j=1}^N \frac{\partial \mathcal{F}_t^{(k)}}{\partial \dot{\zeta}_j} \delta \zeta_j = \frac{\partial \mathcal{F}_t^{(k)}}{\partial \dot{\zeta}_1} \delta \zeta_1 \quad (2.49)$$

The Rayleigh dissipation function is used to represent the viscous damping forces by means of a single scalar. The viscous damping is proportional to the generalized velocities \dot{q}_j and is one of the most important non-conservative forces acting on an aerodynamic surface. Taking this approach to represent the external forces acting on the flexible system, the Lagrange's equation could be also written in this special form:

$$\frac{d}{dt} \frac{\partial \mathcal{L}}{\partial \dot{q}} - \frac{\partial \mathcal{L}}{\partial q} + \frac{\partial \mathcal{F}}{\partial \dot{q}} = Q_{q_0} \quad (2.50)$$

Where Q_{q_0} represents the generalized forces generated by the "frozen" configuration. In this work, when referring to the generalized forces Q_q both "frozen" and viscous damping forces are considered.

Returning on Eq. 2.48 and 2.49, the terms of the Rayleigh's dissipation function relative to wing bending \mathcal{F}_b and torsion \mathcal{F}_t , are defined as:

$$\mathcal{F}_b^{(k)} = \int_0^{l_k} \frac{\partial f_A}{\partial \dot{\xi}} \dot{\xi}^2 dx_k \quad (2.51)$$

$$\mathcal{F}_t^{(k)} = \int_0^{l_k} \frac{\partial M_A}{\partial \theta} \dot{\theta}^2 dx_k \quad (2.52)$$

Which can be both recast in a quadratic form as:

$$\mathcal{F}_b^{(k)} = \dot{\eta}^T C_b^{(k)} \dot{\eta} = \{\dot{\eta}_1 \ \dot{\eta}_2\} [C_b^{(k)}] \begin{Bmatrix} \dot{\eta}_1 \\ \dot{\eta}_2 \end{Bmatrix} \quad (2.53)$$

$$\mathcal{F}_t^{(k)} = \dot{\zeta}^T C_t^{(k)} \dot{\zeta} = \dot{\zeta}_1 [C_t^{(k)}] \dot{\zeta}_1 \quad (2.54)$$

Where the elements of the positive definite matrices $C_b^{(k)}$ and $C_t^{(k)}$ are given by:

$$[C_b^{(k)}]_{i,j} = \frac{1}{2} \int_0^{l_k} \frac{\partial f_{A_k}}{\partial \dot{\xi}_k} \Phi_i(x_k) \Phi_j(x_k) dx_k \quad (2.55)$$

$$[C_t^{(k)}]_{i,j} = \frac{1}{2} \int_0^{l_k} \frac{\partial M_{A_k}}{\partial \dot{\theta}_k} \Psi_i(x_k) \Psi_j(x_k) dx_k \quad (2.56)$$

Therefore, since in this thesis two bending modes are considered, the $C_b^{(k)}$ matrix becomes:

$$\begin{bmatrix} \frac{1}{2} \int_0^{l_k} q_d S c^{(k)} C_{L_\alpha} \left[\frac{1}{u} \right] \Phi_1^2(x_k) dx_k & \frac{1}{2} \int_0^{l_k} q_d S c^{(k)} C_{L_\alpha} \left[\frac{1}{u} \right] \Phi_1(x_k) \Phi_2(x_k) dx_k \\ \frac{1}{2} \int_0^{l_k} q_d S c^{(k)} C_{L_\alpha} \left[\frac{1}{u} \right] \Phi_2(x_k) \Phi_1(x_k) dx_k & \frac{1}{2} \int_0^{l_k} q_d S c^{(k)} C_{L_\alpha} \left[\frac{1}{u} \right] \Phi_2^2(x_k) dx_k \end{bmatrix} \quad (2.57)$$

Where q_d is the dynamic pressure. Regarding the matrix concerning the torsion terms, its derivation is more straightforward, since only one torsional mode is considered:

$$C_t^{(k)} = \int_0^{l_k} \frac{1}{2} \rho V^2 S c^{(k)} C_{L_\alpha} (x_\theta - x_{CA}) \left[\frac{(x_\theta - x_{CA})}{u} \right] \Psi_1^2(x_k) dx_k \quad (2.58)$$

Returning on the expression of the virtual work derived in Eq. 2.35, in the considered case the virtual work of the flexible wing can be expressed as:

$$\delta W = Q_{q_1} \delta q_1 + \dots + Q_{q_n} \delta q_n = Q_{\eta_1} \delta \eta_1 + Q_{\eta_2} \delta \eta_2 + Q_{\zeta_1} \delta \zeta_1 \quad (2.59)$$

Therefore, by means of Eq. 2.46-2.49, the expressions of the generalized forces generated by every considered mode Q_{q_n} can be straightforwardly derived by simply collecting the terms multiplying the virtual displacements expressed in terms of generalized coordinates $\delta \eta_1$, $\delta \eta_2$ and $\delta \zeta_1$.

2.3.4 Flexible Model Conclusion

Now that all the terms of Lagrange's equation are available it is possible to write the equations of motion of the flexible wing. Since in this work only two bending modes and one torsional mode were considered, the complete system is the following:

$$\begin{cases} \frac{d}{dt} \frac{\partial \mathcal{L}}{\partial \dot{\eta}_1} - \frac{\partial \mathcal{L}}{\partial \eta_1} = Q_{\eta_1} \\ \frac{d}{dt} \frac{\partial \mathcal{L}}{\partial \dot{\eta}_2} - \frac{\partial \mathcal{L}}{\partial \eta_2} = Q_{\eta_2} \\ \frac{d}{dt} \frac{\partial \mathcal{L}}{\partial \dot{\zeta}_1} - \frac{\partial \mathcal{L}}{\partial \zeta_1} = Q_{\zeta_1} \end{cases} \quad (2.60)$$

which can be reorganized in the following matrix from:

$$M\ddot{q} + C\dot{q} + Kq = f_q \quad (2.61)$$

where $q = \{\eta_1, \eta_2, \zeta_1\}$ and M is the mass matrix which collects all the terms which multiply the second time derivative of the deformation variables. Similarly, C is the damping matrix and collects all the terms which multiply the first time derivative of the deformation variables. Finally, K is the stiffness matrix and the vector f_q contains all the terms which do not depend on $\{\eta_1, \eta_2, \zeta_1\}$.

2.4 Complete Model

Once the flexible model is fully derived, it can be also used as "correction" to the rigid and aerodynamic models, as shown in Figure 2.1. That means rewriting the aerodynamic loads also in function of the local angle of attack α_w derived in Eq. 2.41, which will influence the equations of the rigid aircraft dynamics together with the elastic deformations. This can be achieved by simply proceeding as follows:

- Impose trim conditions and derive from Eq. 2.61 the generalized coordinates vector $q = \{\eta_1, \eta_2, \zeta_1\}$.
- Once η_1, η_2 and ζ_1 are known, it is possible to determine the elastic deformations ξ_w and θ_w from Eq. 2.31 and 2.32.

At this point it is straightforward to determine the local angle of attack variation due to the wing deformation α_w using Eq. 2.41. The latter can then be used to calculate the new aerodynamic loads which are going to modify the states obtained with the rigid model.

Chapter 3

Gust Model

As stated before, the aim of this thesis is to study the wing behaviour under a gust disturbance. In order to achieve this objective, a proper gust model must be selected. Regulations, as [9] (paragraphs CS 25.341 and AMC 25.341), refer to two different types of gust disturbance models which can be used to determine the loads acting on an aircraft during flight:

- Discrete gust models.
- Continuous gust models.

The first is also referred as an "individual gust" and it is generally an idealization of the gust structure, the second instead aims to represent more accurately the probabilistic nature of atmospheric turbulence.

This chapter is focused on highlighting the differences between the discrete and continuous models, giving particular attention to the latter description through some probability concepts. All of this is largely described in [10], which is the main reference for this chapter. Finally, implementation in the flexible model will be addressed.

However, before diving in the description of these gust models, a brief introduction on gust loads fundamentals may be required.

3.1 Gust Load Introduction

Gust loads, whether due to discrete gusts or continuous turbulence, are ordinarily considered to be the result of a change in angle of attack due to a component of gust velocity at right angles to the flight path. Vertical and lateral gusts fall into this category and the change in angle of attack, in the hypothesis of small perturbations, can be expressed as:

$$\tan(\Delta\alpha) = \frac{U_g}{V} \approx \Delta\alpha \quad (3.1)$$

Where V is the aircraft forward speed and U_g is the gust velocity, as schematized in the example in Figure 3.1.

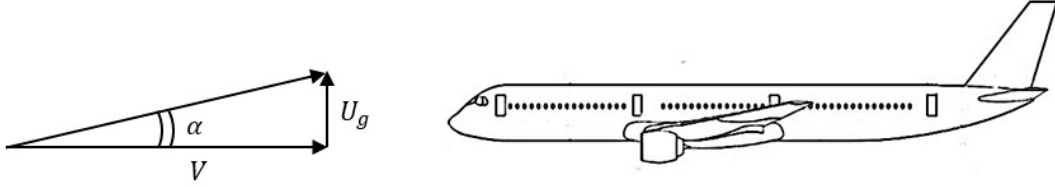


Figure 3.1: Example of Vertical Gust

Considering a vertical gust, the lift variation due to the perturbation can be written as:

$$\Delta L = \frac{1}{2}\rho V^2 SC_{L_\alpha} \Delta\alpha = \frac{1}{2}\rho V^2 SC_{L_\alpha} \frac{U_g}{V} = \frac{1}{2}\rho U_g V SC_{L_\alpha} \quad (3.2)$$

This variation in angle of attack, moreover, affects the aircraft motion. The net change of angle of attack felt by the entire aircraft depends not only on the gust velocity, but also on the aircraft motion induced by the gust itself. Since a gust perturbation will never reach its maximum instantaneously, during the build-up the aircraft will have time to acquire motion. For example, for vertical gust, the aircraft will respond by:

- **Plunging:** the aircraft translates in the direction of the gust velocity, thus the net gust velocity effect is reduced.
- **Pitching:** generally the aircraft, due to its pitch stability, will tend to reduce the increment in angle of attack due to the gust.

This behaviour can be described by writing the differential equation of motion of the rigid aircraft responding to a vertical gust in terms of a single variable α . The variable α represents the increment in angle of attack due to the aircraft motions and it does not include the angle of attack α_g associated with the gust velocity, which is used instead as the forcing function. The result is a second-order differential equation, so the aircraft response to a gust is analogous to that of a mass-spring-damper system. For this reason the aircraft motions can result not only in load alleviation¹, but also in a load increase due to dynamic overshoot.

¹The loads are proportional to $(\alpha_g + \alpha)$, and at low frequencies α tends to subtract from α_g , resulting in a load reduction.

Loads due to lateral gust are affected by aircraft motions similarly to what has just been described for a vertical gust.

However, gust disturbances are not always perpendicular to the aircraft forward speed, but can also be in the same direction, as schematized in Figure 3.2. This perturbation is called head-on gust, and it affects only the dynamic pressure (the angle of attack remains constant).

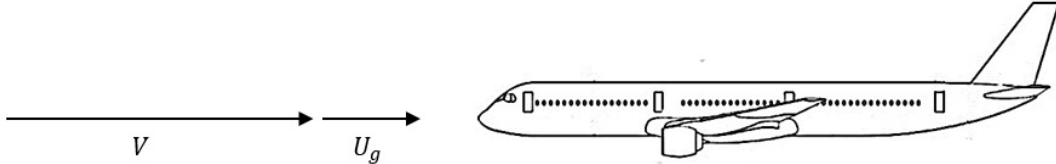


Figure 3.2: Example of Head-on Gust

For this reason, in this case the lift variation due to the perturbation can be written as:

$$\begin{aligned} \Delta L &= \frac{1}{2}\rho[(V + U_g)^2 - V^2]SC_L = \frac{1}{2}\rho[2U_gV + U_g^2]SC_L = \\ &= \frac{1}{2}\rho(2U_gV) \left(1 + \frac{1}{2}\frac{U_g}{V}\right) SC_L \approx \frac{1}{2}\rho(2U_gV)SC_L \quad (3.3) \end{aligned}$$

Note that in this case ΔL depends on steady-flight C_L instead of $C_{L\alpha}$, but still depends on the product U_gV . This means the head-on gust produces only a lift increase, not a side force or a change in the aircraft attitude directly.

This lift variation affects also the aircraft motion. For a head-on gust, the alleviation effect of plunge motion is the same as for a vertical gust; the motion will depend only on the lift produced, not on its source. The pitch motion instead will be different, as the increment in lift due to a vertical gust will act at the aircraft aerodynamic center, whereas the lift due to a head-on gust will act at the l-g flight center of pressure, that is, the CG. These can differ substantially, for example as the result of a difference between wing and tail angles of attack in l-g flight. In addition, head-on gust could lead to a small alleviation effect due to the slowdown resulting from the drag increase associated with the dynamic pressure increase.

3.2 Discrete Vs. Continuous Gusts

In this thesis when referring to a gust profile a gust velocity time history is intended. Typically, gust profiles tend to be continuous and irregular, as in the example shown in Figure 3.3. Generally, when the profile is continuous, the gust structure is referred

to as turbulence, whereas when the gust structure consists of more or less isolated pulses, the single pulse is referred to as a gust. Also, a continuous turbulence profile can be thought as a series of individual gusts.

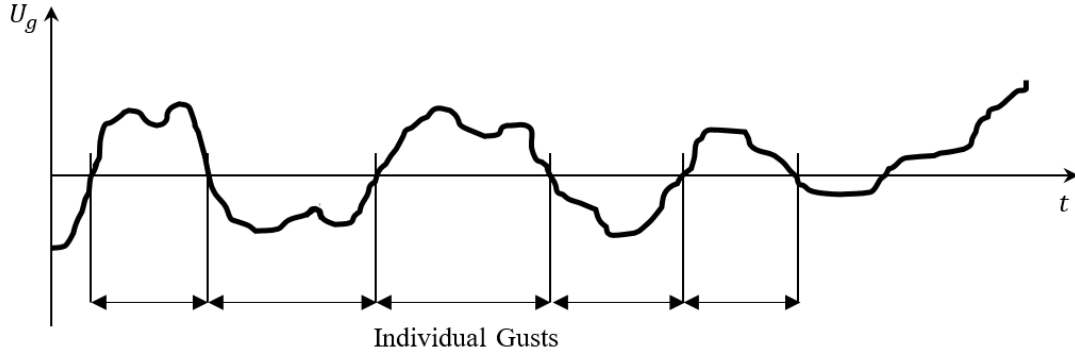


Figure 3.3: Example of Gust Profile

The usual individual gust, or discrete gust, idealization of the gust structure, reported also in CS 25 regulation, consist in a "1 - cos" ("one-minus-cosine") pulse, as shown in Figure 3.4.

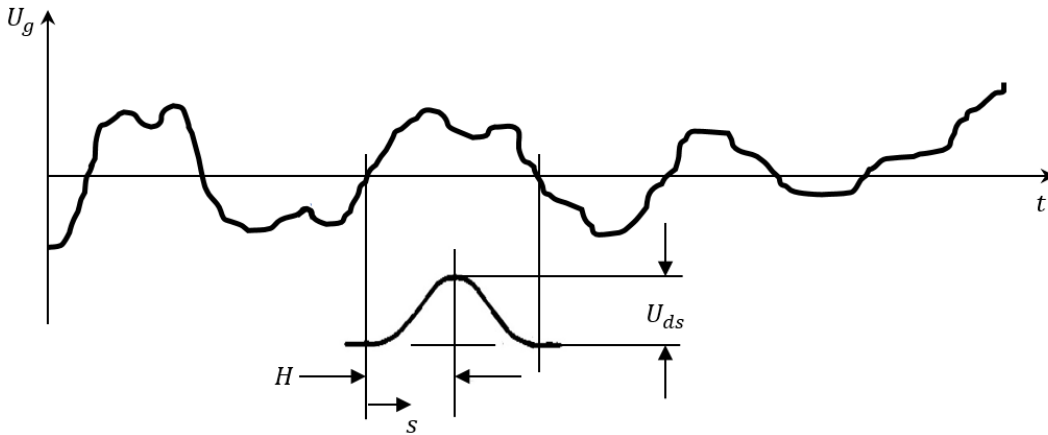


Figure 3.4: "1 - cos" Discrete Gust Idealization

Mathematically, the shape of the gust is described as follows:

$$U_g = \begin{cases} \frac{U_{ds}}{2} \left[1 - \cos \left(\frac{\pi s}{H} \right) \right] & 0 < s \leq 2H \\ 0 & s > 2H \end{cases} \quad (3.4)$$

Where s represents the distance penetrated in to the gust; H is the gust gradient, which is the distance parallel to the aircraft flight path for the gust to reach its peak

velocity (ranges between 9m and 107m). Lastly, U_{ds} is the design gust velocity in equivalent airspeed, given by the following formula:

$$U_{ds} = U_{ref} F_g \left(\frac{H}{107} \right)^{1/6} \quad (3.5)$$

In which, U_{ref} represents the reference gust velocity in equivalent air speed, indicated by CS 25 regulation as a function of altitude for a gust gradient H of 107m. Finally, F_g represents the flight profile alleviation factor. In defining the value of U_{ref} at each altitude, it is assumed that the aircraft is flown 100% of the time at that altitude. The factor F_g is applied to account for the expected service experience in terms of the probability of the aeroplane flying at any given altitude within its certification altitude range. F_g value is minimum at sea level, linearly increasing to 1.0 at the certified maximum altitude. At sea level, F_g can be determined by the following equation:

$$F_g = 0.5 (F_{gz} + F_{gm}) \quad (3.6)$$

Where:

$$F_{gz} = 1 - \frac{Z_{mo}}{76200} \quad (3.7)$$

$$F_{gm} = \sqrt{R_1 \tan \left(\frac{\pi R_2}{4} \right)} \quad (3.8)$$

$$R_1 = \frac{MLW}{MTOW} \quad (3.9)$$

$$R_2 = \frac{MZFW}{MTOW} \quad (3.10)$$

In which Z_{mo} is the aircraft maximum operating altitude, MLW is the maximum landing weight, $MTOW$ is the maximum take-off weight and $MZFW$ is the maximum zero fuel weight.

The "1 - cos" gust idealization is a straightforward method to represent atmospheric turbulence acting on an aircraft during flight and thus an "easy-to-use" tool to determine gust loads within a good approximation. For this reason is included in both military and civil regulations and must be taken in consideration during aircraft design.

However, it does not represent well the continuous and irregular nature of gust profiles, as represented in the example in Figure 3.3. For this reason gust profiles are often idealized as "stationary Gaussian random processes". With this method, the profile is considered stationary, that means it is considered of infinite duration and its statistical properties are the same wherever it may be sampled. The gust time

history it is also Gaussian, because if it is sampled at random, the resulting probability distribution is Gaussian (or "normal") and defined by a probability density function:

$$p(y) = \frac{1}{\sqrt{2\pi}\sigma_y} e^{-\frac{1}{2}\left(\frac{y}{\sigma_y}\right)^2} \quad (3.11)$$

where σ_y is constant. Finally the term "random" indicates that the profile has no apparent pattern or regularity, thus it can be defined only in terms of its statistical characteristics.

This idealization is vastly more realistic than the simple discrete-gust idealizations. In fact, it provides:

- Infinite shape variation of the individual gusts.
- Variation of gust magnitude with the gust gradient distance H .
- Proper superposition of short-gradient gusts, that excite the various elastic modes, with the longer-gradient gusts, that give the largest rigid-aircraft loads.
- The reduced gust velocity properly associated (on an equal-probability basis) with a resonant series of gusts.

In addition, several mathematical techniques are available to use this idealization, as generalized harmonic analysis or power-spectral analysis. These permit to determine the statistical characteristics of the aircraft response (accelerations, loads, etc.) directly from the statistical description of the gust velocity profile. For this reason, before describing the most used continuous gust models, in section 3.3 some probability and PSD² concepts are given.

3.3 Probability and PSD Concepts

First of all, a measure of the magnitude of the continuous gust profile must be determined. Let y be any stationary random function of time, as the gust time history in Figure 3.3. The magnitude of the fluctuations of y over its mean value, can be measured by its RMS³ value σ_y , defined as:

$$\sigma_y = \sqrt{y^2} = \sqrt{\lim_{T \rightarrow \infty} \frac{1}{2T} \int_{-T}^T [y(t)]^2 dt} \quad (3.12)$$

²Power Spectral Density

³Root-Mean-Square

in which the "bar" over y denotes the average. This equation applies only when the mean value of y is zero. If it is not then, for the purpose of Eq. 3.12, y has to be taken as an increment to its mean value. For example if y is, instead of the gust velocity, the aircraft response, y is taken to be the increment relative to the 1-g level flight value. To evaluate σ_y from a time history, the time history can be read at small uniform intervals, or it can be sampled randomly, as represented in Figure 3.5. In either case, Eq. 3.12 becomes:

$$\sigma_y = \sqrt{\overline{y^2}} = \sqrt{\lim_{N \rightarrow \infty} \frac{1}{N} \sum_{i=1}^N [y(t_i)]^2} \quad (3.13)$$

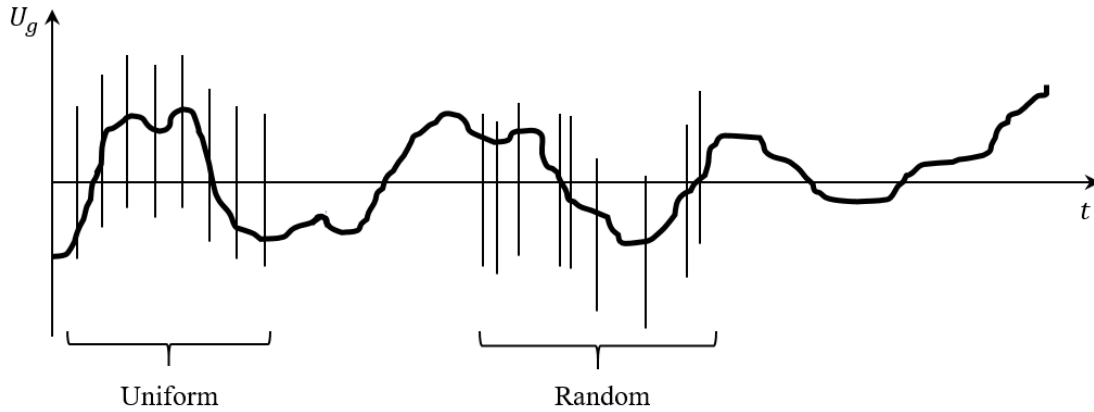


Figure 3.5: Example of Gust Sampling

Note that y is squared before averaging because otherwise positive and negative fluctuations will offset each other to give a value of zero. Thus, the purpose of measuring the magnitude of the fluctuations of y would be defeated.

Other two important concepts to better understand the magnitude of y are the probability density and the probability distribution. The probability density $p(y)$ is defined as the quantity such that, in any trial, the probability that y lies between y_1 and $y_1 + dy$ is equal to the area of the element $p(y_1)dy$, as shown in Figure 3.6. The term y_1 is a particular value of y . In the example in Figure 3.6, $p(y)$ is symmetrical about $y = 0$. This symmetry is characteristic of a stationary Gaussian random process but is not necessary in general.

The probability distribution $P(y)$, schematized in Figure 3.7, is defined as the probability that $y < y_1$, and its given by:

$$P(y) = \int_{-\infty}^{y_1} p(y)dy \quad (3.14)$$

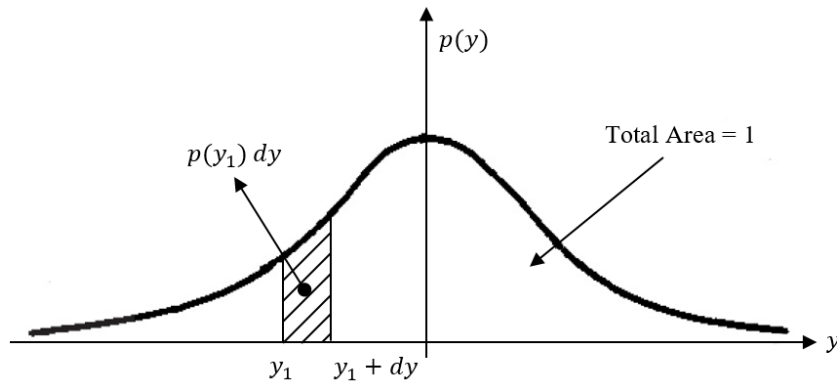


Figure 3.6: Probability Density

Another way to define the probability distribution is the function $1 - P(y)$, which is the probability that y is greater than y_1 :

$$1 - P(y) = \int_{y_1}^{\infty} p(y) dy \quad (3.15)$$

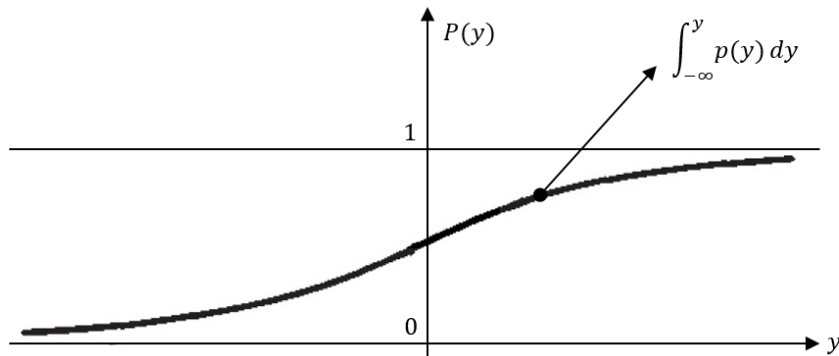
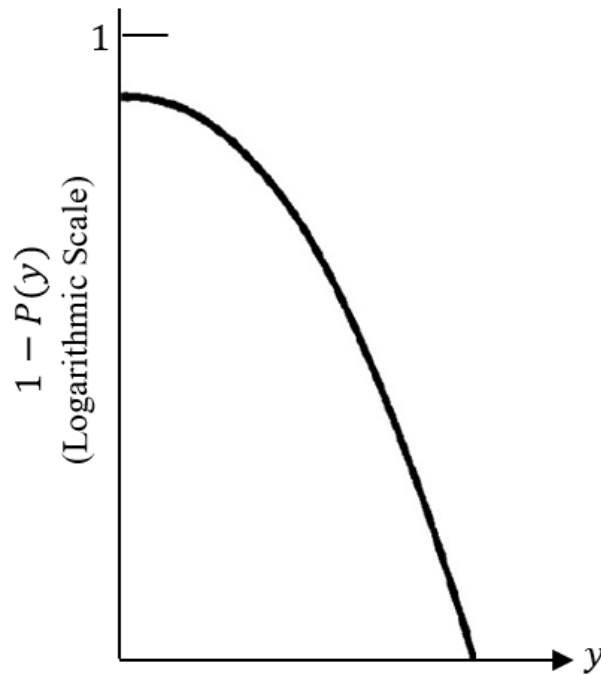


Figure 3.7: Probability Distribution

Graphically $1 - P(y)$ plot can be obtained simply by mirroring Figure 3.7 around the ordinate axis, but it is usually plotted in semi-logarithmic scale, as reported in Figure 3.8.

This form of plot is especially useful in connection with selection of design values of y , especially for values that are exceeded with low probability. For example, a value of 0.00026, is simpler both to understand and plot than 0.99974. Also, it permits to express the value of y as a two-significant-figure number instead of a five-significant-figure one.

Figure 3.8: $1 - P(y)$ in Logarithmic Scale

As already stated in section 3.2, a particular probability distribution of great importance for continuous gust modelling is the Gaussian probability distribution. This is defined by the probability density given by Eq. 3.11, where σ_y is the RMS value of y . Note, again, that y is the difference between y and its mean: if y is taken as the quantity itself, it should be replaced with $(y - y_{mean})$ in Eq. 3.11. Graphically, Figure 3.6 shows an example of Gaussian probability density.

Importance of normal distributions is partly due to the central limit theorem, which states that, under some conditions, the average of many samples (observations) of a random variable with finite mean and variance (defined as σ_y^2) is itself a random variable whose distribution converges to a normal distribution as the number of samples increases. For this reason, Gaussian distributions are often used to represent real-valued random variables whose distributions are not known, such as continuous gust velocities.

In loads applications, an additional requirement is that the probability density of \dot{y} is also Gaussian and \dot{y} has to be independent of y . An alternate way to express this requirement is that the process has to be "joint Gaussian", which means that the joint probability density of y_1 and y_2 , where y_1 and y_2 are values of y separated by a given time increment τ , has to be Gaussian. A joint probability density is defined analogously to a single variable probability density, thus is expressed as the

probability that x is between x and $x + dx$ and at the same time y is between y and $y + dy$ is $p(x, y)dxdy$, where:

$$p(x, y) = \frac{1}{2\pi\sigma_x\sigma_y\sqrt{1-r^2}} \exp \left\{ -\frac{1}{1-r^2} \left[\frac{1}{2} \left(\frac{x}{\sigma_x} \right)^2 - r \left(\frac{x}{\sigma_x} \right) \left(\frac{y}{\sigma_y} \right) + \frac{1}{2} \left(\frac{y}{\sigma_y} \right)^2 \right] \right\} \quad (3.16)$$

It can be demonstrated that if this more fundamental requirement is met, then the previously stated additional requirement, that \dot{y} be Gaussian, is also met.

The practical importance of any additional requirement, over and above the one that the distribution of y itself has to be Gaussian, is that is necessary in the derivation of Rice's equation. Rice's equation is the basis for the analytical determination of frequency of exceedance curves, which are used to apply the probabilistic nature of the atmospheric turbulence directly as loads on the structure. In practice, the probability distribution of any load quantity y , expressed in the form $1 - P(y)$, can be thought as equivalent to the fraction of time, over a very long sample, that y will be in excess of y_1 . However, this probability tells nothing at all about the probability that a maximum peak within some finite time interval, will be in excess of a certain y_1 . Nor does it indicate the number of peaks to be expected, in excess of various values of y_1 within the same time interval. For this kind of information, frequency of exceedance data is needed. Although this is not this thesis objective, is noticeable how the data given by this approach is useful in the determination of the aircraft load spectrum, thus in the fatigue sizing of structural components.

Recapping what has been said so far, the magnitude of a stationary Gaussian random process is defined statistically by its RMS value and its probability distribution (Gaussian). In order to complete the statistical description of the random process, it is required, in addition, the definition of its frequency content.

A stationary Gaussian random process can be considered to be generated by the superposition of an infinite number of sinusoidal components, which differ infinitesimally in frequency (ω) from one to the next. Also, each component is of prescribed infinitesimal amplitude and each is randomly phased relative to the others. Mathematically this can be expressed as:

$$y(t) = \sum_{m=1}^{\infty} \underbrace{\sqrt{\Phi(\omega_m)\Delta\omega}}_{\text{Inf. Amplitude}} \cos(\omega_m t + \underbrace{\Psi_m}_{\text{Random Phase}}) \quad (3.17)$$

How sinusoids superimpose to form a stationary Gaussian random process is illustrated in the example in Figure 3.9. Note that a sum of a limited number of sinusoids has already the appearance of a stationary Gaussian random process.

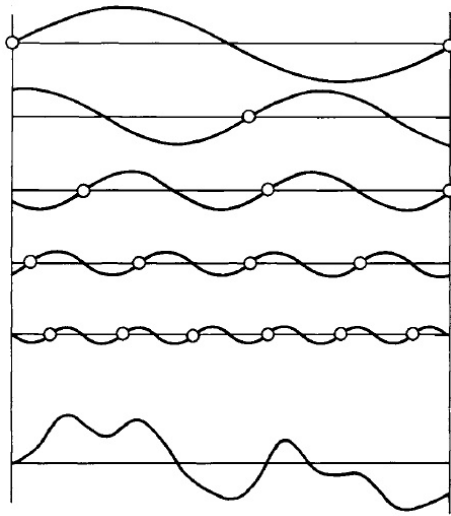


Figure 3.9: Example of Superimposition of Sinusoids

Returning on Eq. 3.17, the term $\Phi(\omega_m)$ is called the PSD of the process, which, as a continuous function of frequency ω , provides the complete measure of the frequency content of the process. Physically speaking, if $\Phi(\omega)$ is the PSD of the quantity $y(t)$, then $\Phi(\omega)d\omega$ is the contribution to $\overline{y^2}$ (or σ_y^2) of frequencies between ω and $\omega + d\omega$ (Figure 3.10). In terms of RMS this can be expressed as:

$$\sigma_y = \sqrt{\int_0^{\infty} \Phi(\omega) d\omega} \quad (3.18)$$

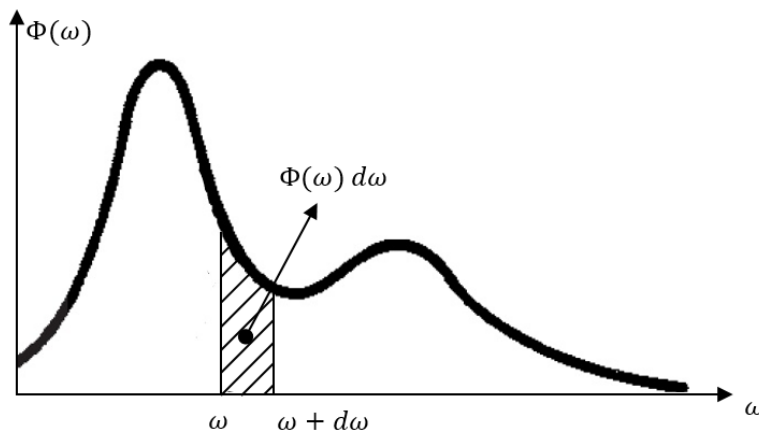


Figure 3.10: PSD Scheme

Given $\Phi(\omega)$, an infinite number of time histories can be generated by means of Eq. 3.17. Conversely, given a time history a single PSD can be calculated. This could be done, for example, using the "autocovariance function", defined as:

$$R(\tau) = \overline{y(t)y(t+\tau)} = \lim_{T \rightarrow \infty} \frac{1}{2T} \int_{-T}^T y(t)y(t+\tau) dt \quad (3.19)$$

This expresses the correlation of a function with itself ("auto") at points separated by various times τ . For $\tau = 0$, $R = \overline{y^2} = \sigma_y^2$, quantity which in statistics is often referred as "variance". The PSD can be determined from $R(\tau)$ as follows:

$$\Phi(\omega) = \frac{2}{\pi} \int_0^{\infty} R(\tau) \cos \omega\tau dt \quad (3.20)$$

Conversely:

$$R(\tau) = \int_0^{\infty} \Phi(\omega) \cos \omega\tau dt \quad (3.21)$$

Equations 3.20 and 3.21 are a special form of Fourier transform. This is only an example of how determine a PSD from a time history. A more effective way, in terms of computational cost, is given by the Fast Fourier Transform method (FFT), which is not covered in this thesis.

In general, given a gust PSD, two types of approach can be followed to determine the gust response of an aircraft. One consist in to use the gust PSD to generate a gust velocity time history, which its then used to perturb the aircraft model. This method is the one selected for this thesis and it is described in Section 3.4. The other approach consist in to use the gust PSD (input) to determine the PSD of the aircraft response (output), and will be briefly described below.

For a linear system, with subscripts i and o denoting input and output, the input spectrum (Φ_i) is multiplied, frequency by frequency, by the square of the modulus of the frequency-response function (transfer function), to give the output spectrum:

$$\Phi_o(f) = \Phi_i(f) |H(f)|^2 \quad (3.22)$$

The output probability distribution, if the input probability distribution is Gaussian, will also be Gaussian. The output RMS value is given by the square root of the area under the output PSD curve, as given by Eq. 3.18.

In gust loads applications, the transfer function is obtained by solution of the differential equations of motion of the aircraft: the input is a sinusoidally varying (steady state) gust velocity, and the various outputs are the corresponding sinusoidally varying shears, bending moments, torsions, accelerations, concentrated inertia forces, and/or whatever else may be of interest.

This approach can be useful, for example, to determine if and how much gust loads increase due to structural flexibility. It is sufficient to determine the frequency

response function for both the rigid and the flexible aircraft. Then use those to calculate, for example, both flexible and rigid bending moment PSD by means of Eq. 3.22. Therefore it is possible to calculate, using Eq. 3.18, the RMS of the output PSD. The ratio of flexible-aircraft to rigid-aircraft bending moments is then given by the ratio of the RMS values, thus obtaining a ratio between both bending moments magnitude. This approach, using a von Kármán's vertical gust PSD shape as input (described in Section 3.4), is basically the one presented in CS-25 regulation for continuous gust loads determination.

However this method requires the system to be linear in order to determine its transfer function and thus applying Eq. 3.22. Since the aircraft model presented in this thesis is expressed by a non-linear system, this gust load determination method based on PSD is not suitable for this work.

3.4 Dryden and von Kármán Turbulence Models

Two continuous gust, or turbulence, models have been widely used in aircraft design and simulation applications: those are the Dryden and von Kármán models. Both models define the linear and angular velocity components of continuous gusts as stationary Gaussian random processes and specify each component PSD by means of mathematical expressions. Both of these models PSD and the procedures related to them are reported in [13], [28] and [29].

For the head-on gust velocity u_g , the corresponding PSD $\Phi_u(\omega)$ is defined as:

$$\begin{array}{cc}
 \textit{Dryden} & \textit{von Kármán} \\
 \frac{2\sigma_u^2 L_u}{\pi V} \cdot \frac{1}{1 + \left(L_u \frac{\omega}{V}\right)^2} & \frac{2\sigma_u^2 L_u}{\pi V} \cdot \frac{1}{\left[1 + \left(1.339 L_u \frac{\omega}{V}\right)^2\right]^{5/6}} \quad (3.24)
 \end{array} \quad (3.23)$$

For vertical and lateral gust velocities w_g and v_g , the corresponding PSD $\Phi_w(\omega)$ and $\Phi_v(\omega)$ are the same and are defined as:

$$\begin{array}{cc}
 \textit{Dryden} & \textit{von Kármán} \\
 \frac{2\sigma_w^2 L_w}{\pi V} \cdot \frac{1 + 12 \left(L_w \frac{\omega}{V}\right)^2}{\left[1 + 4 \left(L_w \frac{\omega}{V}\right)^2\right]^2} & \frac{2\sigma_w^2 L_w}{\pi V} \cdot \frac{1 + \frac{8}{3} \left(2.678 L_w \frac{\omega}{V}\right)^2}{\left[1 + \left(2.678 L_w \frac{\omega}{V}\right)^2\right]^{11/6}} \quad (3.26)
 \end{array} \quad (3.25)$$

As mentioned above, these models specify also angular velocity components PSD.

Since the flexible model presented in this thesis takes in consideration only the aircraft longitudinal dynamics, only the pitch rate PSD $\Phi_q(\omega)$, which is the same for both Dryden and von Kármán models, is here reported:

$$\Phi_q(\omega) = \frac{\pm \left(\frac{\omega}{V}\right)^2}{1 + \left(\frac{4b\omega}{\pi V}\right)^2} \cdot \Phi_w(\omega) \quad (3.27)$$

In both military and civil regulations, these PSD are expressed in terms of spatial frequency Ω , instead of circular frequency ω , which can be written as:

$$\Omega = \frac{\omega}{V} \quad (3.28)$$

Where V is the speed with which the aircraft is moving through the gust field. Therefore, the PSD in terms of spatial frequency are expressed as:

$$\Phi_i(\Omega) = V\Phi_i(\omega) \quad (3.29)$$

Other terms appearing in the PSD equations are the turbulence intensity σ_i , which is the gust component RMS, and the turbulence scale length L_i . This latter variable, in practice, determines the frequency at which the knee of the PSD curve occurs: in other words, L_i influences the shape of the PSD curve, as shown in Figure 3.11. This implies that the value of L_i should be chosen so that the resulting gust PSD fits, as closely as possible, the actual turbulence that the aircraft will encounter. However, as pointed in Figure 3.11, for values of $L \geq 1000$ ft, the turbulence scale length affects the RMS value without changing the curves in the region of frequencies where the aircraft develops load.

For this reason, in civil aircraft design, for gust load determination purposes L_i tend to be selected as constant: CS-25 regulation takes L_i equal to 2500 ft for all altitudes, while the gust RMS is changed and scaled with a F_g factor, which is the same of Eq. 3.6 pointed in Section 3.2.

However, for altitudes less than about 2500 ft above the ground, the scale of turbulence probably tends to be less, especially for the vertical component. This is surely important for high-speed flight at low altitudes but also when modelling the aircraft landing. For this reason, military regulations attempt to reflect this turbulence reduction specifying a low-altitude model ($h \leq 1000$ ft) and a medium/high-altitude model ($h \geq 2000$ ft).

For altitudes less than 1000 ft, the turbulence scale length for both Dryden and von Kármán is taken as:

$$2L_w = h \quad (3.30)$$

$$L_u = 2L_v = \frac{1}{(0.177 + 0.000823h)^{1.2}} \quad (3.31)$$

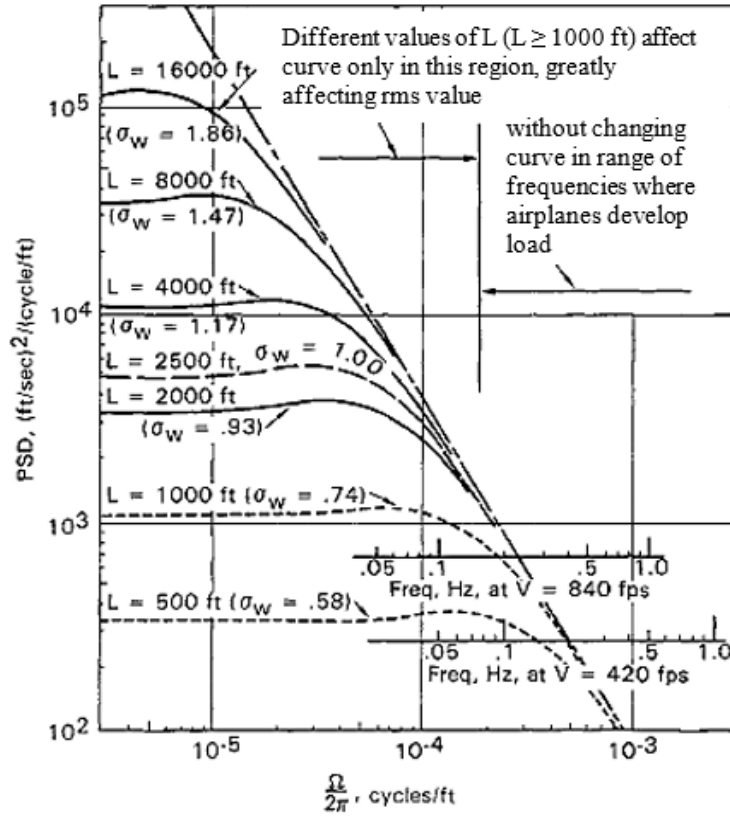


Figure 3.11: Effect of L on PSD

The fact that longitudinal turbulence scale length is twice as great then the vertical and lateral ones is obtained experimentally by expressing L_i in terms of the autocovariance function (Eq. 3.19), as follows:

$$L = \frac{\int_0^\infty R(\tau) dt}{R(0)} \quad (3.32)$$

The turbulence intensities σ_i instead, are given, again for both models as:

$$\sigma_w = 0.1W_{20} \quad (3.33)$$

$$\frac{\sigma_u}{\sigma_w} = \frac{\sigma_v}{\sigma_w} = \frac{1}{(0.177 + 0.000823h)^{0.4}} \quad (3.34)$$

Where W_{20} is the wind speed at 20 ft, which is typically 15 knots for light turbulence, 30 knots for moderate turbulence and 45 knots for severe turbulence. Note that, at low altitudes, wind speed is taken in wind axes, thus a direction cosine matrix must be defined to rotate the gust velocities in body axes.

For altitudes above than 2000 ft, the turbulence scale length is taken as:

Dryden

von Kármán

$$L_u = 2L_v = 2L_w = 1750\text{ft} \quad (3.35) \quad L_u = 2L_v = 2L_w = 2500\text{ft} \quad (3.36)$$

The turbulence intensities instead have the same value in all directions and are determined from a lookup table that provides the turbulence intensity as a function of altitude and the probability of the turbulence intensity being exceeded. This table is derived from the graphic in Figure 3.12. The turbulence axes orientation in this altitude region is defined as being already aligned with the body coordinates.

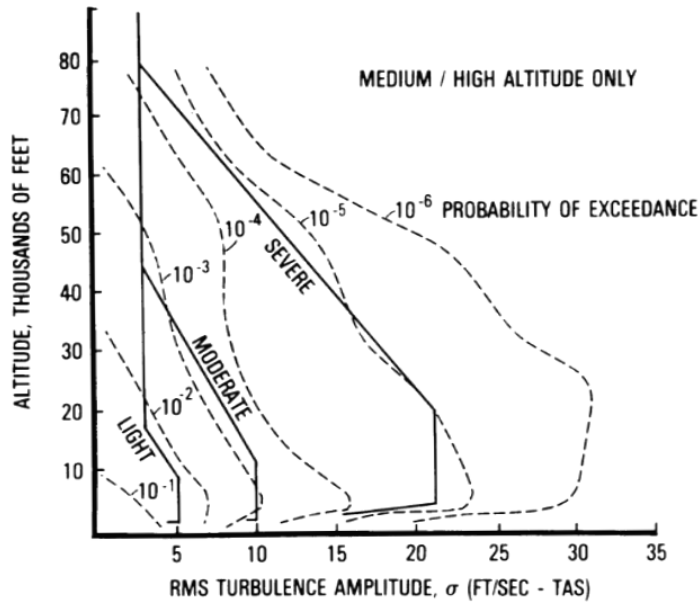


Figure 3.12: Medium/High Altitude Turbulence Intensities

Finally, for altitudes between 1000 ft and 2000 ft the turbulence velocities and turbulence angular rates are determined by linearly interpolating between the value from the low altitude model (transformed in body coordinates) and the value from the high altitude model.

At this point it remains to explain how to recreate a gust velocity time history starting from a gust PSD given by Dryden or von Kármán model. This can be done by passing a band limited white noise⁴ through a forming filter derived from the

⁴In signal processing, white noise is a random signal having equal intensity at different frequencies, giving it a constant power spectral density.

gust PSD. This leads to an output signal with the same PSD of the chosen model, which can be used as wind disturbance. For Dryden's PSD, an exact filter can be derived from the spectral square roots of the spectrum equations (spectral factorization process). For von Kármán's PSD, the desired filter can only be approximated. For the longitudinal gust component, the filter $H_u(s)$ is given by:

$$\begin{array}{ccc}
 \text{Dryden} & & \text{von Kármán} \\
 \sigma_u \sqrt{\frac{2L_u}{\pi V}} \cdot \frac{1}{1 + \frac{L_u}{V}s} & (3.37) & \frac{\sigma_u \sqrt{\frac{2L_u}{\pi V}} \left(1 + 0.25 \frac{L_u}{V}s\right)}{1 + 1.357 \frac{L_u}{V}s + 0.1987 \left(\frac{L_u}{V}\right)^2 s^2} \quad (3.38)
 \end{array}$$

For the vertical and lateral gust components, the filters $H_w(s)$ and $H_v(s)$ are given by:

$$\sigma_w \sqrt{\frac{L_w}{\pi V}} \cdot \frac{1 + \sqrt{3} \frac{L_w}{V}s}{\left(1 + \frac{L_w}{V}s\right)^2} \quad \text{Dryden} \quad (3.39)$$

$$\frac{\sigma_w \sqrt{\frac{2L_w}{\pi V}} \left(1 + 2.7478 \frac{2L_w}{V}s + 0.3398 \left(\frac{2L_w}{V}\right)^2 s^2\right)}{1 + 2.9958 \frac{2L_w}{V}s + 1.9754 \left(\frac{2L_w}{V}\right)^2 s^2 + 0.1539 \left(\frac{2L_w}{V}\right)^3 s^3} \quad \text{von Kármán} \quad (3.40)$$

Finally, for the pitch rate angular velocity gust component, the filter $H_q(s)$ for both Dryden and von Kármán models is defined as:

$$H_q(s) = \frac{\pm \frac{s}{V}}{\left(1 + \left(\frac{4b}{\pi V}\right)s\right)} \cdot H_w(s) \quad (3.41)$$

Knowing these filters expressions allows to, since a white noise is by definition a random signal, generate an infinite number of gust time histories witch share the same PSD.

Speaking of the two turbulence models here presented, the von Kármán gives the better fit to observed data and for this reason it is the standard for design use. The Dryden model has retained its importance primarily because of the ease of deriving the filter needed to generate a proper gust time history.

Regarding model implementation, the Matlab/Simulink Aerospace Blockset provides already a block containing both Dryden and von Kármán models as described above. An example of moderate continuous turbulence time history for the vertical

gust velocity component, generated using the von Kármán model block in Simulink, is shown in Figure 3.13.

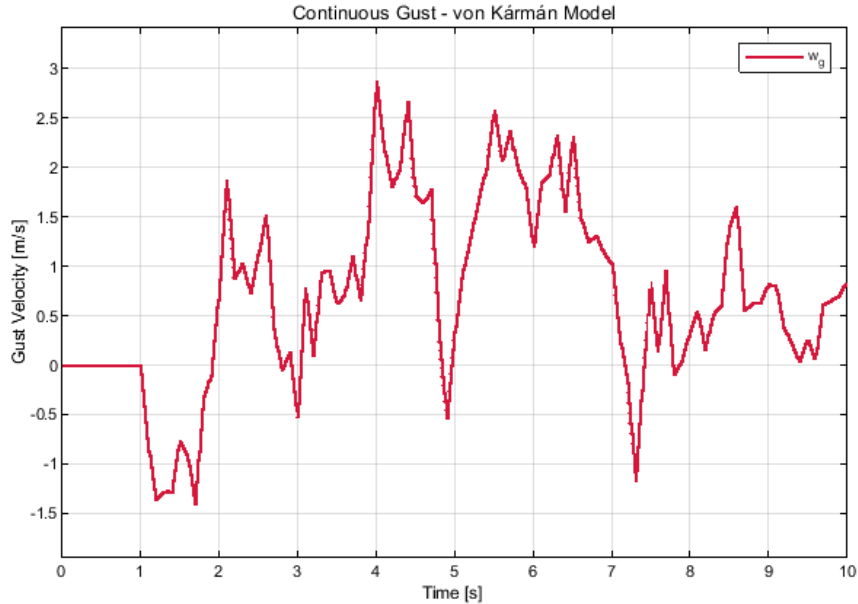


Figure 3.13: Continuous Gust Example

Once the gust time history is obtained, two approaches can be followed to implement it as disturbance in the model. The first is to derive the variation over time of the angle of attack due vertical gust perturbation by means of Eq. 3.1. Then use it as external perturbation of the angle of attack obtained by the rigid model. However, this approach does not take in consideration an eventual head-on or pitch rate perturbation. This is acceptable in terms of civil aircraft regulation, since CS-25 gives requirements only on vertical and lateral gusts.

A second method is to consider the gust velocities as direct perturbation of the rigid ones inside of the aircraft rigid model. This permits to consider all the desired velocities, although it is formally incorrect since, by definition, a gust is an external disturbance. However, this approach permits to consider different gust perturbations at the same time, giving possibly a more realistic atmospheric turbulence behaviour.

In either case, gust disturbances act firstly on the rigid model which then influences, as explained in Chapter 2, the flexible behaviour of the aircraft by means of Lagrange's equations (Section 2.3).

Chapter 4

Wing Response & Load Determination

Having defined a gust model, it is possible to use the resulting velocity time histories to perturb the rigid aircraft model. The rigid model response, in turn, influences the flexible wing response in terms of bending, torsion and their relative rates by means of Lagrange's equation, as explained in Section 2.3.

Knowing how the wing reacts to an external perturbation, anyway, does not give directly any information on the loads this perturbation has generated on the flexible structure. Load determination is important in both aircraft structural analysis, which is largely performed via FEM¹ simulations, and in control system design, especially for GLA² purposes.

Generally, dynamic flexible aircraft models, as the one presented in this work, can not leave aside completely a prior FEM analysis of the flexible structure, since data needed in the model as, for example, shape functions and Young's modulus of every considered airframe section are not easily computable without having an accurate structural model. Anyway, although determining loads by means of a FEM analysis leads to more accurate results, this approach introduces significant complication both in calculations and in the model definition.

For this reason, in this chapter two approaches for gust load determination are presented and compared. The first is directly linked to the flexible model as presented in Section 2.3.4, whereas the second is linked to the strip theory. While the first it is more accurate but dependant from some FEM data as explained above, the second requires some approximations and simplifications, but also does not necessarily require FEM data in order to determine the flexible loads.

¹Finite Element Method

²Gust Load Alleviation

Furthermore, the first part of this chapter will show the wing response to discrete and continuous gusts in terms of flexible accelerations, in order to give a complete overview of how an external perturbation influences flexible dynamics.

4.1 Wing Response

In order to analyse the generic flexible wing response to a gust perturbation, a proper model, following the theory addressed in Chapter 2, was implemented using Matlab/Simulink software. Some general wing geometry data and the aircraft mass used in the model are shown in Table 4.1. The model considers the aircraft being in

Wing Geometry & Aircraft Mass	
Wing Span	29.65 m
Mean Aerodynamic Chord	2.56 m
Wing Surface	73.28 m ²
Aircraft Mass	20147 kg

Table 4.1: General Aircraft Data

cruise phase with an OEW³ mass configuration. The aerodynamic force and moment coefficients are calculated using classical flight mechanics linear expressions:

$$C_L = C_{L_0} + C_{L_\alpha} \alpha + (C_{L_\alpha} \dot{\alpha} + C_{L_q} q) \frac{\bar{c}}{V} + C_{L_{\delta_e}} \delta_e + C_{L_{\delta_a}} (\delta_{a_R} + \delta_{a_L}) \quad (4.1)$$

$$C_M = C_{M_0} + C_{M_\alpha} \alpha + (C_{M_\alpha} \dot{\alpha} + C_{M_q} q) \frac{\bar{c}}{V} + C_{M_{\delta_e}} \delta_e \quad (4.2)$$

$$C_D = C_{D_0} + kC_L^2 + C_{D_{\delta_a}} (\delta_{a_R} + \delta_{a_L}) \quad (4.3)$$

In which \bar{c} is the mean aerodynamic chord and the subscripts R and L denote respectively right and left wing. Furthermore, these coefficients are considered reliable under the following hypotheses:

- Mach number $M \leq 0.3$
- Angle of Attack $0^\circ < \alpha < 4^\circ$
- Maximum deflection of control surfaces $\pm 10^\circ$

³Operative Empty Weight

Also note that the aileron deflection derivative here accounted is referred to the symmetric activation of the control surfaces, since, as already stated in Section 2.1, only the longitudinal aircraft dynamics are considered in the presented model.

Regarding the flexible part of the model, the wing is considered divided in 30 sections and mounted to the aircraft with null dihedral and sweep angles. Shape functions values were approximated idealizing the wing as a cantilever beam.

Once the initial data is defined, the flexible model is applied as explained in Section 2.3. The obtained system of Lagrange's equations (Eq. 2.60) is then reorganized in the matrix form shown in Eq. 2.61. This "mass-spring-damper" configuration of the flexible dynamics equations permits to easily determine the accelerations of the wing sections in terms of generalized coordinates:

$$\{\ddot{q}\} = [M]^{-1} [\{f_q\} - [C] \{\dot{q}\} - [K] \{q\}] \quad (4.4)$$

Where is recalled that $q = \{\eta_1, \eta_2, \zeta_1\}$ is the generalized coordinates vector, f_q is the vector containing the terms related to the rigid dynamics and thus not dependant on the wing deformation and M , C and K are respectively the mass, damping and stiffness matrices of the flexible system.

The generalized coordinates vector can be determined by integrating \ddot{q} two times consecutively. This integration can be done by using quadrature methods, as for example, the trapezoidal rule or its composite variant.

Once the generalized coordinates vector is obtained, the actual wing deflection and torsion of each section are easily determinable by multiplying each mode amplitudes by the respective shape function, as shown in Eq. 2.31 and 2.32. The same approach can be applied to determine the flexible velocities and accelerations from \dot{q} and \ddot{q} .

Following this approach is thus possible determining the wing response to a gust disturbance or to a command.

Firstly, the wing response to an elevator step is evaluated. This type of command is useful to highlight the differences between the wing response in terms of acceleration and deformation rates, which are not appreciable when analysing more gradual perturbations, as discrete or continuous gusts. Figures 4.1 and 4.2 show respectively bending and torsion rates, while Figures 4.3 and 4.4 show the respective accelerations. All the results are scaled in percentage of the maximum peak occurred during the simulation and are given for three different wing sections: wing root section, a mid wing section and the wing tip section.

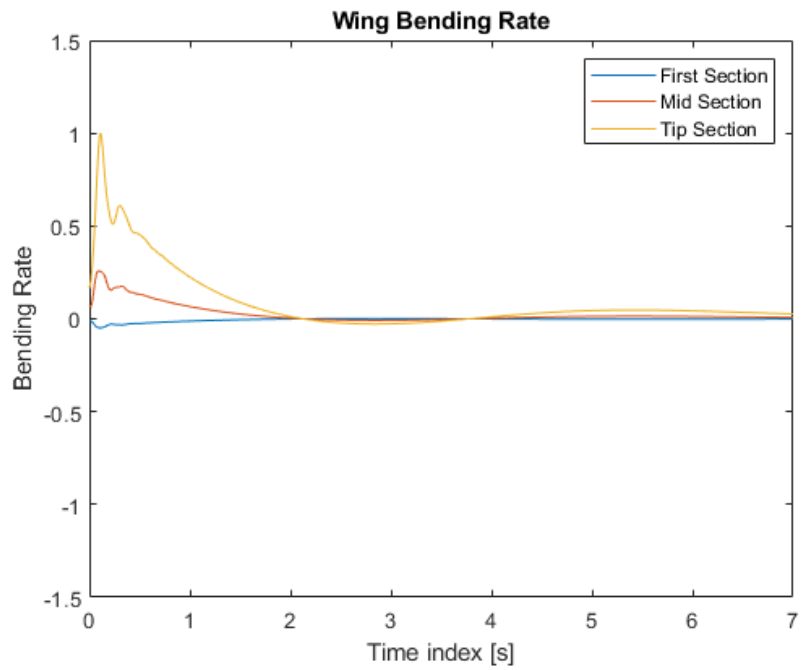


Figure 4.1: Wing Bending Rate after an Elevator Step

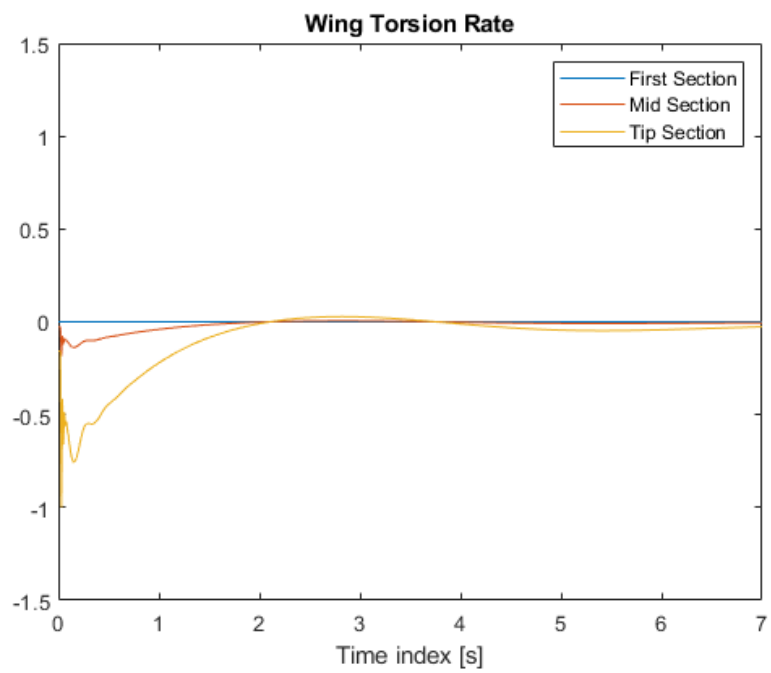


Figure 4.2: Wing Torsion Rate after an Elevator Step

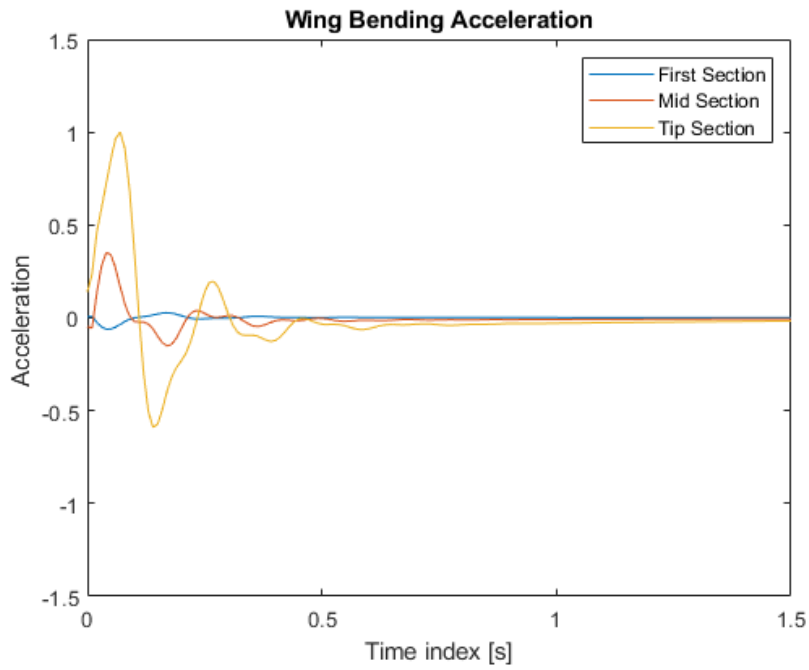


Figure 4.3: Wing Bending Acceleration after an Elevator Step

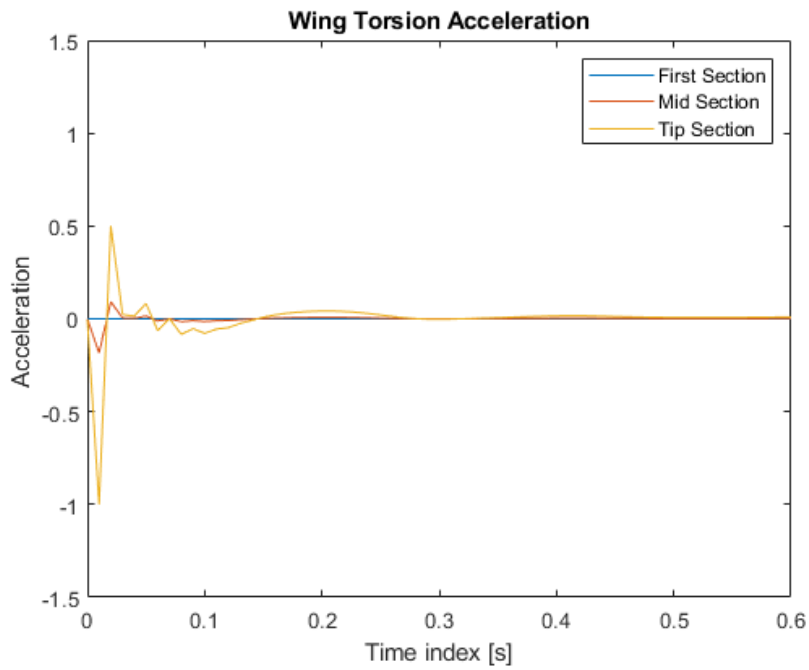


Figure 4.4: Wing Torsion Acceleration after an Elevator Step

In these graphs is already visible how torsional response is in general more "noisy" when compared to bending response. This is given to the grater stiffness along the wing chord, which results in a more oscillatory response. Also in Figure 4.4 it is clear how this grater torsional stiffness generates numerical issues when an instantaneous perturbation, as a step command, is evaluated.

The first analysed perturbation is a "1 - cos" vertical discrete gust as described in Eq. 3.4, having:

$$H = 26 \text{ m} \quad U_{ref} = 17.07 \frac{\text{m}}{\text{s}}$$

The obtained gust profile is shown in Figure 4.5. This gust velocity is then used to describe the perturbation in terms of angle of attack:

$$\alpha_g \approx \frac{w_g}{V} \quad (4.5)$$

which is in turn used in the rigid dynamics equations to perturb the aircraft:

$$\alpha_{AC} = \alpha_{RIG} + \alpha_g \quad (4.6)$$

The graphs in Figure 4.6 and Figure 4.7 show respectively the wing response in terms of bending and torsion accelerations. Again, the results are referred to three wing section and scaled in percentage of the maximum occurred peak.

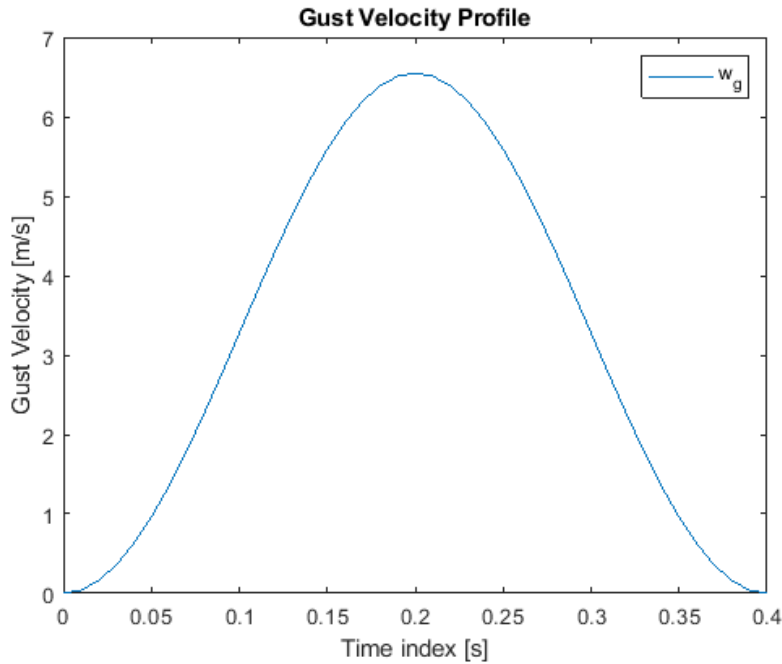


Figure 4.5: "1 - cos" Gust Profile

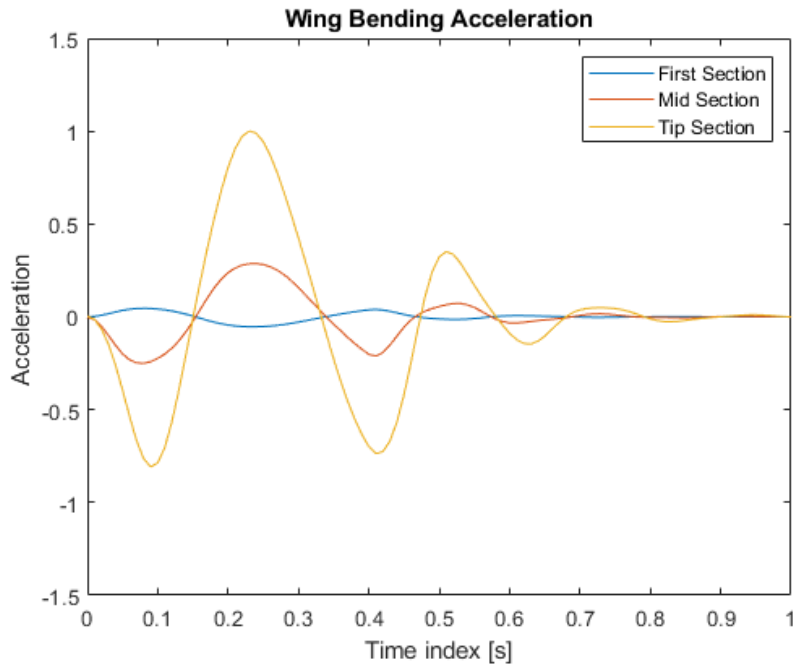


Figure 4.6: Wing Bending Acceleration after a "1 - cos" Gust

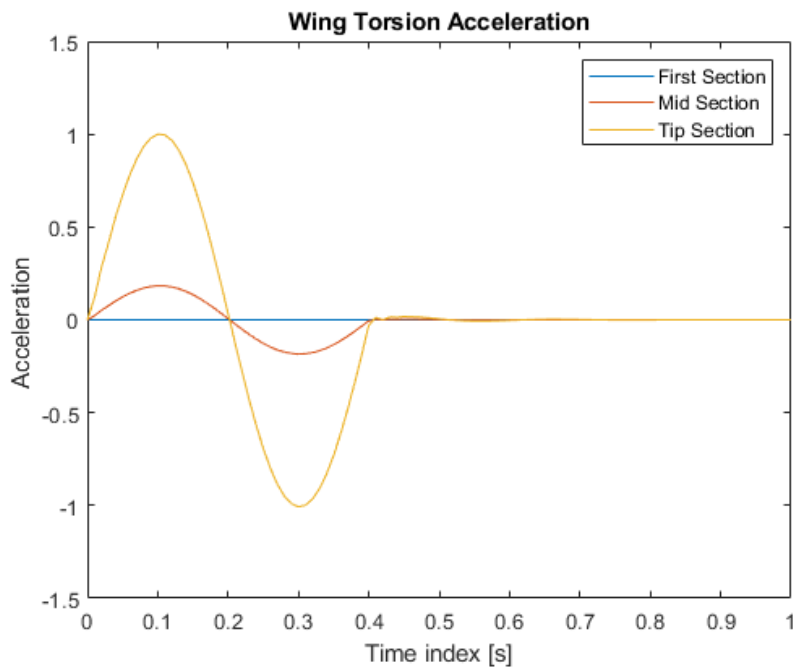


Figure 4.7: Wing Torsion Acceleration after a "1 - cos" Gust

Another analysed perturbation consist in a von Kármán continuous vertical gust shown in Figure 4.8. As reported in Section 3.4, since the model considers the aircraft being in cruise, the turbulence scale length is set to 2500 ft. The turbulence intensity (RMS) is set to "moderate" which corresponds to a probability of exceedance of 10^{-3} as shown in Figure 3.12. The wing response is again reported in terms of flexible acceleration and scaled in percentage of the maximum peak, as shown in Figure 4.9 and Figure 4.10. Both graphs show only the first part of the turbulence, in order to give a more clear view of the wing response.

Comparing the obtained results, is immediately visible the irregular nature of the wing response after a continuous randomly generated gust, especially when compared to the discrete gust response, which shows a typical second order dynamic system trend. Although continuous gust gives a more accurate representation of the atmospheric turbulence, its "noisy" nature makes sometimes the results difficult to read, especially if the analysed system has high stiffness, as for the wing torsion response. In fact in Figure 4.10 is visible how every gust velocity peak generates a "stand-alone" response which is immediately dumped until another peak is reached. This phenomena does not occur with the bending acceleration since the wing stiffness along the wing span is smaller than along the wing chord. In general, continuous gusts are uses to excite the various elastic modes, while discrete gusts are used to generate and study large loads on the structure.

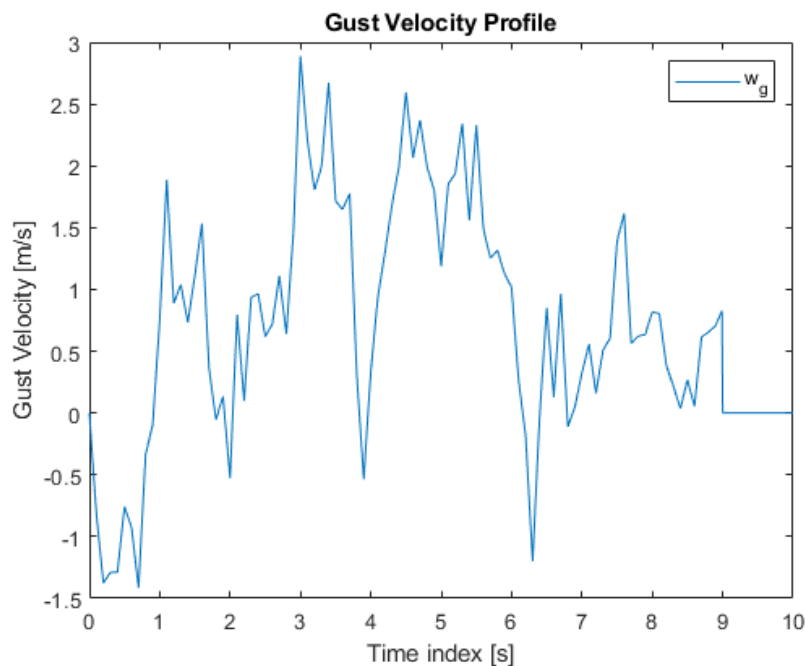


Figure 4.8: Continuous von Kármán Gust Profile

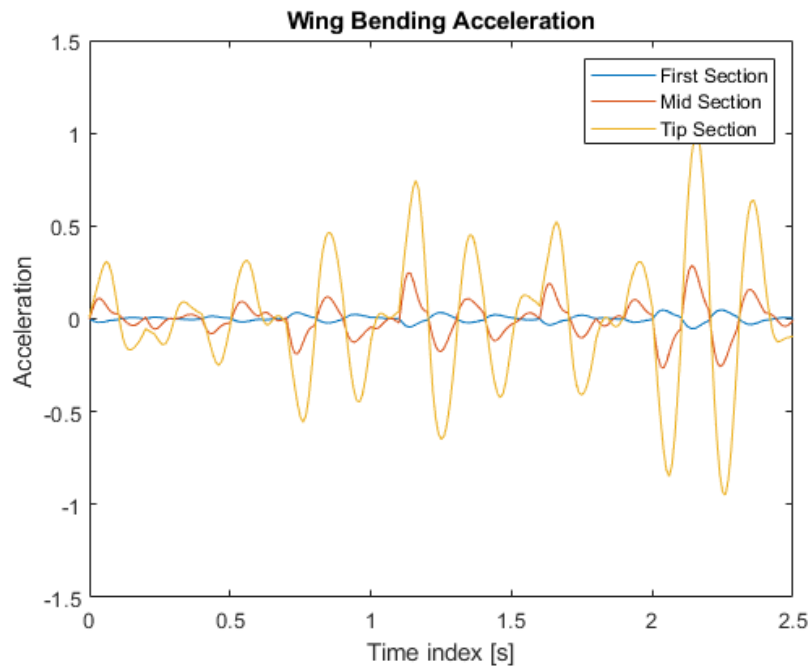


Figure 4.9: Wing Bending Acceleration after a von Kármán Gust

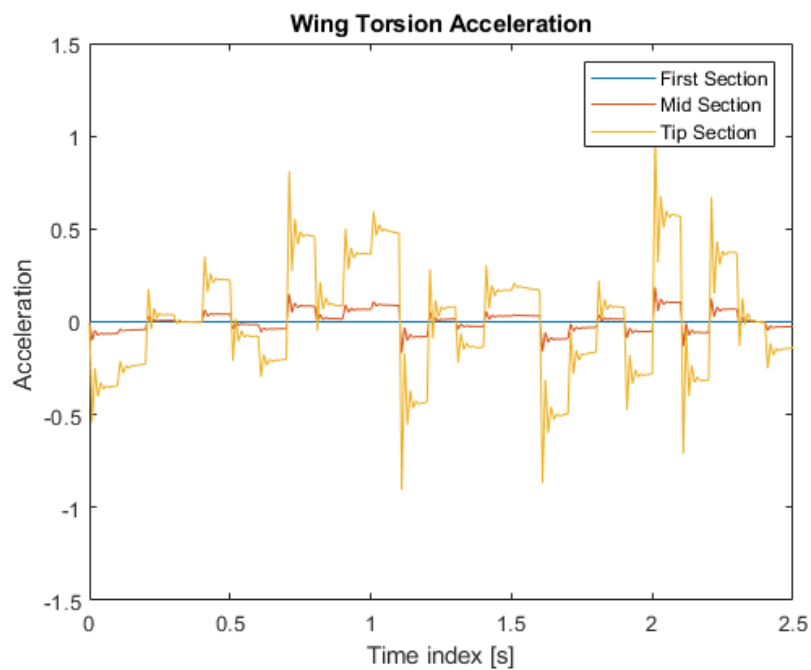


Figure 4.10: Wing Torsion Acceleration after a von Kármán Gust

4.2 Load Determination

4.2.1 MCK Method

Following the model presented in Section 2.3, an accurate method to determine the flexible loads is given by Eq. 2.61. Since an external gust is used to perturb the aircraft, the matrix form of the Lagrange's equations system can be rewritten as:

$$M\ddot{q} + C\dot{q} + Kq = f_{q_0} + f_g \quad (4.7)$$

Where f_g represents the vector of elastic loads generated by the external perturbation in terms of generalized coordinates. This component appears in the equation since, as explained in section 2.3.3, external aerodynamic forces can be expressed as sum of the load generated by the current values of transport and deformation variables ("frozen" configuration) and the load increment generated by the deformation rates. The term f_g represents this load increment over the "frozen" loads of the trim conditions f_{q_0} . In practice, f_g represents the loads terms given by the Rayleigh dissipation function as expressed in Eq. 2.48 and 2.49. Having already defined the entire system, the elastic loads can be easily obtained as follows:

$$f_g = f_{q_0} - (M\ddot{q} + C\dot{q} + Kq) \quad (4.8)$$

However, from Eq. 4.8, f_g is still expressed in terms of generalized coordinates and thus it has to be properly multiplied by the shape function of every considered wing element k :

$$f_{a_g}^{(k)} = f_{g_{\eta_1}} \Phi_1^{(k)} + f_{g_{\eta_2}} \Phi_2^{(k)} \quad (4.9)$$

$$M_{a_g}^{(k)} = f_{g_{\zeta_1}} \Psi_1^{(k)} \quad (4.10)$$

The terms $f_{a_g}^{(k)}$ and $M_{a_g}^{(k)}$ represent respectively the aerodynamic force and the aerodynamic moment generated by the wing deformation on the k -th wing element. These loads are expressed in terms of the aerodynamic chord of the considered section and thus can be seen as distributed loads over the wing span, as schematized in Figure 4.11.

Therefore, the bending moment generated by the wing deflection calculated at the wing root can be expressed as follows:

$$M_{bending} = M_{y_w} = \sum_{k=1}^N \int_0^{x^{(k)}} f_{a_g}^{(k)} x_w^{(k)} dx = \sum_{k=1}^N f_{a_g}^{(k)} \frac{x_w^{2(k)}}{2} \quad (4.11)$$

Similarly, the torsion moment, since it is also distributed over the wing span, can be calculated at the wing root as follows:

$$M_{torsion} = M_{x_w} = \sum_{k=1}^N M_{a_g}^{(k)} x_w^{(k)} \quad (4.12)$$

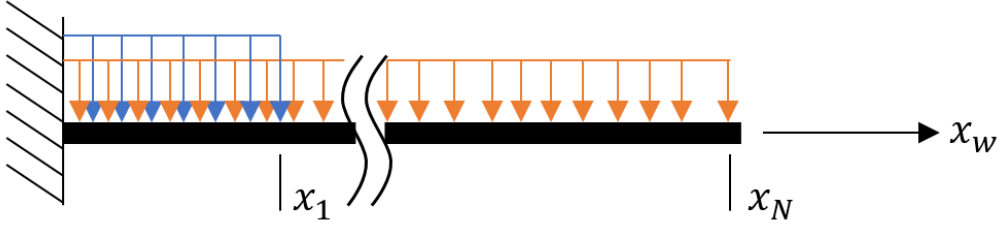


Figure 4.11: Distributed Loads Over The Wing Span

Following this approach it is thus possible to determine the wing loads, in terms of wing bending and torsion moment, starting directly from the "MCK" definition of the system. This is convenient if a model of the flexible dynamics is available, which requires several structural terms that are given from a previous structural analysis. However, in the event that the only available information is the wing response in terms of deformations and relative deformation rates, the MCK method results difficult to apply, and therefore an alternative approach must be found.

4.2.2 Strip Theory

Another, even more simple, method for load determination is given by the strip theory as described in Section 2.2. Neglecting 3D effects associated with finite elongation wings, the aerodynamic loads are expressible in terms of local angle of attack variation of every considered wing section. This angle of attack, as already stated in Section 2.3.3, can be expressed in terms of rigid and flexible variables and, in the hypothesis of small perturbations, is defined as follows:

$$\alpha_w \approx \alpha_{WB} + i_w(x_w) - \frac{q}{u} x_F(x_w) + \frac{\dot{\xi}_w(x_w, t)}{u} + \theta_w(x_w, t) + \frac{\dot{\theta}_w(x_w, t)(x_\theta - x_{CA})}{u} \quad (4.13)$$

Where again x_F represents the distance between the aerodynamic centre of the considered section and the aircraft CG in body reference frame and $(x_\theta - x_{CA})$ represents the distance between the torsion axis and the airfoil aerodynamic center. Note that the spatial derivative of the wing deflection ξ'_w does not influence the local angle of attack, but it generates a small rotation of the lift vector around the y_w axis of the wing reference frame. However, in this case, since the deformations are small, the effect of this rotation can be neglected.

Therefore, knowing α_w and C_{L_α} of the considered wing element it is possible to determine its C_L :

$$C_L(\alpha_w, x_w) = C_{L_\alpha}(x_w)\alpha_w(x_w) \quad (4.14)$$

And thus C_D by the following quadratic relation:

$$C_D(\alpha_w, x_w) = C_{D_0} + k (C_L(\alpha_w, x_w))^2 \quad (4.15)$$

With:

$$k = \frac{1}{\pi \frac{b^2}{S} e} \quad (4.16)$$

In which e is the Oswald factor, in this case taken as 0.9. At this point, knowing the lift and drag coefficients it is possible to determine the aerodynamic force coefficient C_Z of the considered wing section:

$$C_Z(\alpha_w, x_w) = -C_L(\alpha_w, x_w) \cos \alpha_w - C_D(\alpha_w, x_w) \sin \alpha_w \quad (4.17)$$

At this point it is possible to easily determine the aerodynamic force and moment acting on every wing section as follows:

$$f_{Aw} = \frac{1}{2} \rho V^2 c(x_w) C_Z(\alpha_w, x_w) \quad (4.18)$$

$$M_{Aw} = \frac{1}{2} \rho V^2 c(x_w) C_Z(\alpha_w, x_w) (x_\theta - x_{CA}) \quad (4.19)$$

These loads as well are expressed in terms of the aerodynamic chord of the considered section and thus can be seen as distributed loads over the wing span. Therefore bending and torsion moments at the wing root can be expressed by means of Eq. 4.11 and Eq. 4.12, equally to the loads determined with the MCK method.

4.3 Results Comparison

This section is dedicated to show and compare the results given by the two methods presented in Section 4.2. Figures 4.12 and 4.13 represent respectively bending and torsion moments at wing root generated by an elevator step. Both graphs are referred to the loads generated by only the deformation rates, in order to eliminate the loads associated with the "frozen" trim configuration and make the MCK and strip theory methods comparable. For this reason, in the least method, the angle of attack given by Eq. 4.13 was reduced considering only the deformation rates $\dot{\xi}_w$ and $\dot{\theta}_w$. In the same way, Figures 4.14 and 4.15 represent respectively bending and torsion moments at wing root generated by the "1 - cos" discrete gust shown in Figure 4.5. Concluding, Figures 4.16 and 4.17 show bending and torsion moment generated by the deformation rates only after the von Kármán continuous gust represented in Figure 4.8.

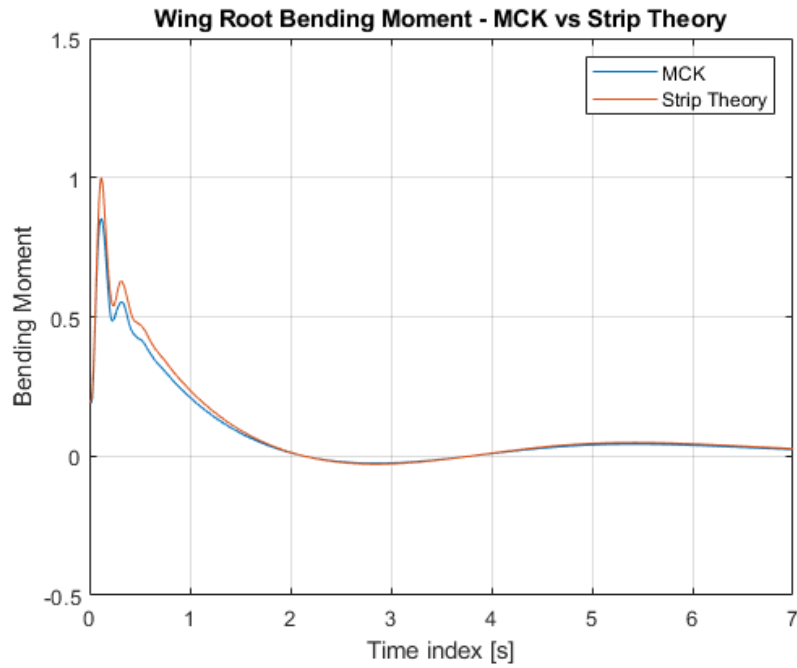


Figure 4.12: Wing Root Bending Moment - Deformation Only - Step of δ_e

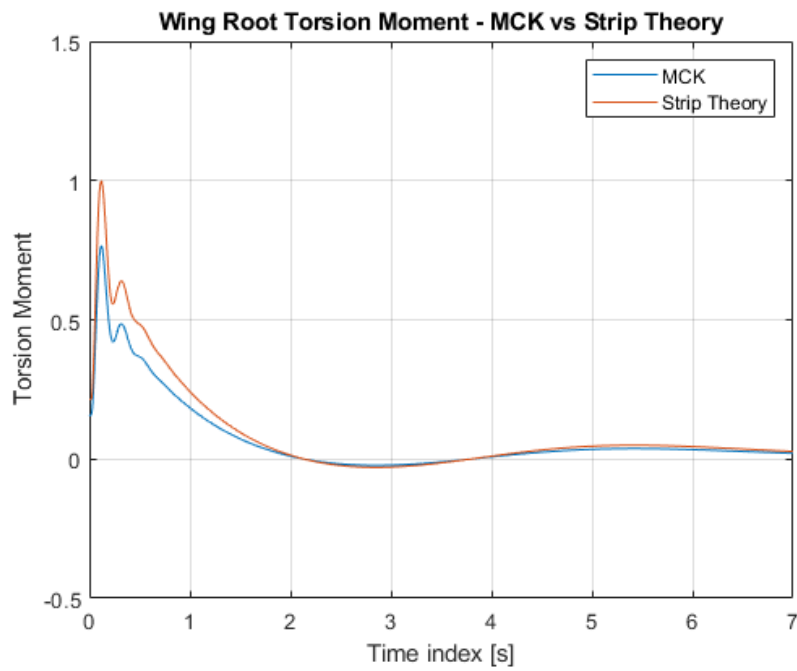


Figure 4.13: Wing Root Torsion Moment - Deformation Only - Step of δ_e

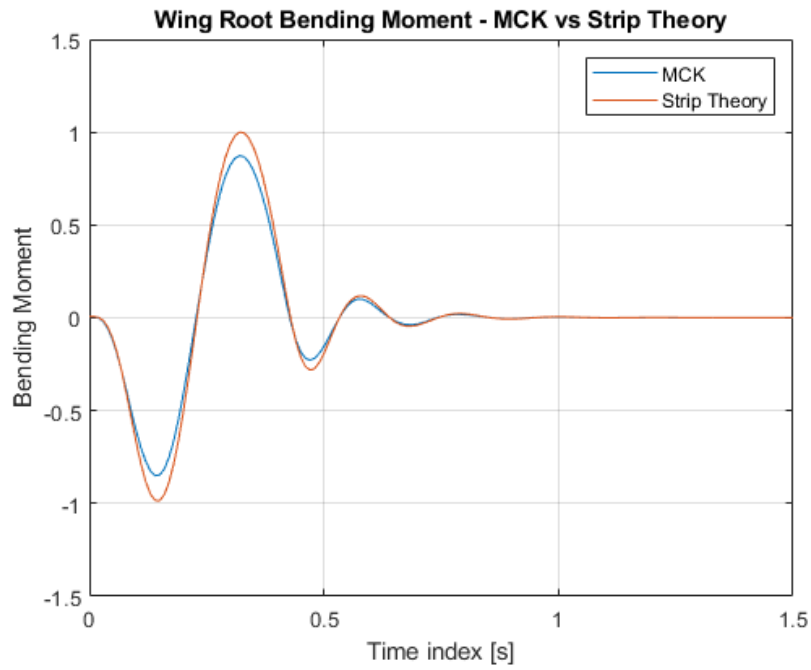


Figure 4.14: Wing Root Bending Moment - Deformation Only - " $1 - \cos$ "

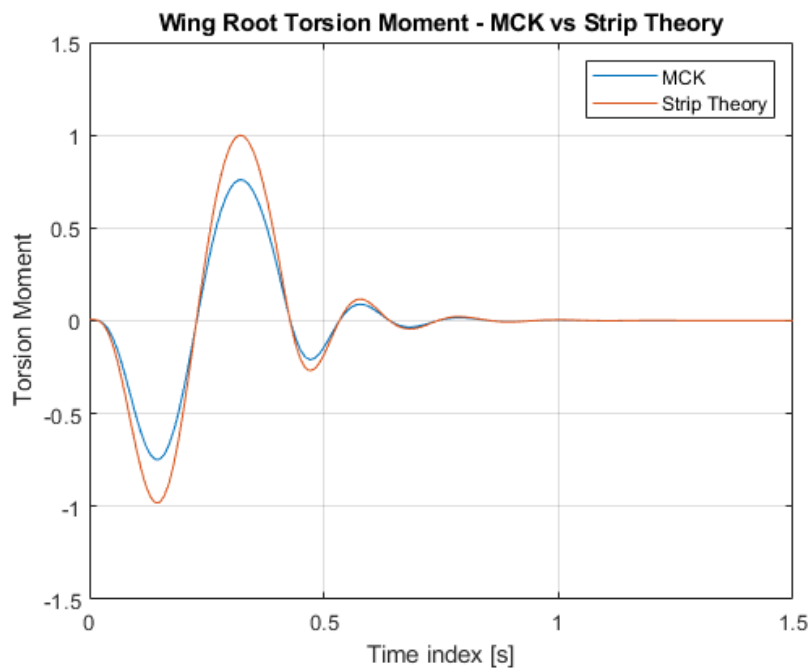


Figure 4.15: Wing Root Torsion Moment - Deformation Only - " $1 - \cos$ "

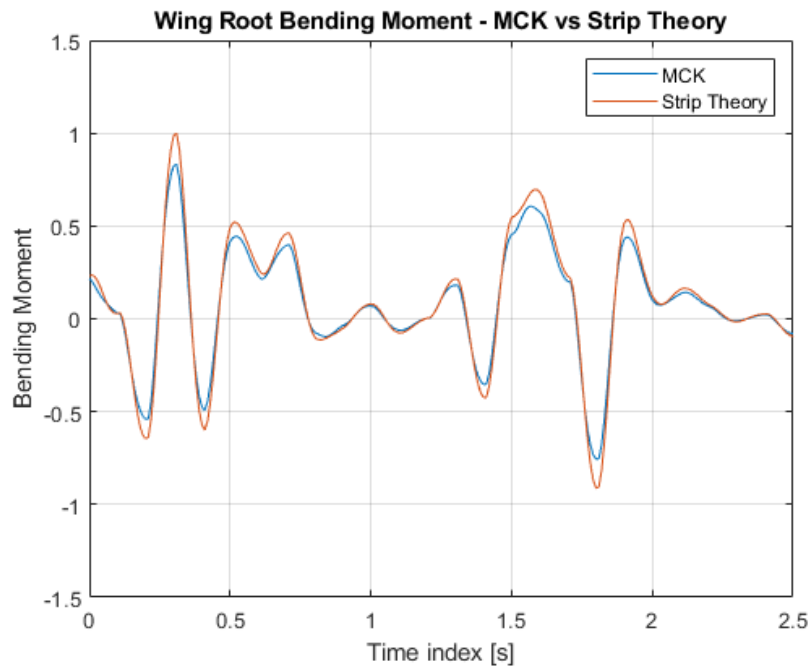


Figure 4.16: Wing Root Bending Moment - Deformation Only - von Kármán

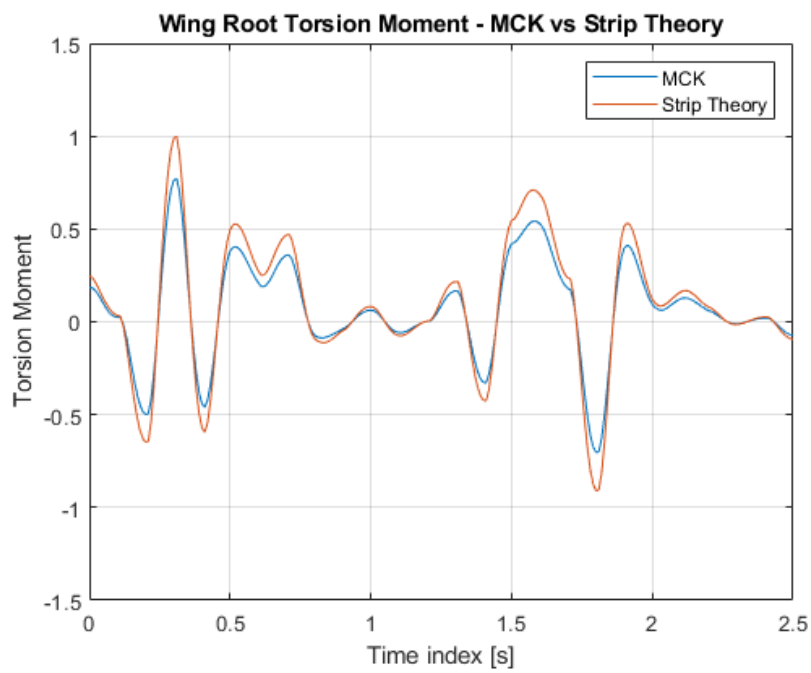


Figure 4.17: Wing Root Torsion Moment - Deformation Only - von Kármán

For all the considered perturbations, results were again scaled to the maximum peak occurred during the simulations. In all graphs it is visible how the results obtained with the strip theory are less damped than the ones obtained with the "MCK" method, especially for the torsion load. This happens because the strip theory takes all structural information from only the deformation rates, and thus this clearly results in an approximation of the structural loads, and particularly of the structural damping. In any case, the difference between the two methods is about 5%-13% at the bending load peak and 15%-20% at the torsional load peak.

Both of the methods here proposed bring several simplifications and limitations with them:

- C_{L_α} is the only aerodynamic derivative considered to determine the flexible dynamic loads, thus neglecting all the other aerodynamic effects. Also this derivative should be calculated for every considered wing section in order to guarantee more accurate results.
- Due to the model definition, these methods consider only the aircraft longitudinal dynamics effects.
- Load determination accuracy is heavily influenced by the number of wing sections considered, since the aerodynamic loads along the wing span are approximated as a superimposition of the distributed loads generated by these sections. If the number of wing stations is excessively limited, the reconstruction of the loads may be not accurate.

Furthermore, the strip theory method is valid only if the wing is the only considered flexible surface of the aircraft. If other components, as for example the fuselage, are considered flexible, this simplified method would not be suitable for determining the loads of the whole aircraft, and thus other methods must be found. However, this method allows to have an almost accurate estimation of the dynamic loads acting on the wing without necessarily having a prior FEM model. The deformation rates used to determine the local angle of attack (Eq. 4.13) can be obtained directly by means of sensors placed on desired wing stations. This represents an advantage since, in this case, a prior structural analysis to determine data as, for example, the shape functions of the considered wing sections are not needed. However, the strip theory represents a further approximation over the MCK method, which is preferable if a flexible model is already available.

Chapter 5

Control System Design

The last part of this thesis will focus on the design of a control system able to reduce the dynamic loads determined in Chapter 4. As already mentioned before, this loads are generated by the flexible wing response to an external perturbation: therefore, controlling the wing deformation, and, in particular, deformation rates, permits to influence the loads acting on the surface.

However, applying an effective controller directly in the flexible variables is not simple and requires a large amount of data concerning the flexible structure. For this reason, the control strategy proposed in this thesis consist in acting on the rigid aircraft response to an external perturbation, in order to indirectly reduce the flexible structure response and thus the generated dynamic loads.

This can be done by means of a Linear Quadratic Regulator (LQR) acting on both elevator deflections and symmetric aileron deflections. However, this controller can be applied on LTI¹ systems, and thus a linear state-space definition of the model must be defined.

So at beginning of this chapter, a linear state-space definition of the aircraft longitudinal dynamics is given. This is done by means of dimensional derivatives, following the approach reported in [30].

Then a description of the LQR controller theory, as reported in Reference [31], from the cost function definition to the Algebraic Ricatti Equation (ARE) is given, in order to better understand its implementation in the aircraft model.

Finally, the last part of the chapter will be dedicated to display the results in terms of reduction of the aerodynamic loads generated by both discrete and continuous gust. This loads will be determined with the MCK method reported in Section 4.2.1, since this is the more accurate method of the two presented in this work.

¹Linear Time-Invariant

5.1 State-Space System Definition

To proceed with the LQR controller design, the rigid aircraft model must be defined as an LTI system as follows:

$$\dot{x} = Ax + Bu \quad (5.1)$$

Where A is the state matrix, x is the state vector, B is the control matrix and u is the control vector. Since only the longitudinal dynamics are considered in the aircraft model, the state vector is composed of only four elements:

$$x = \{u, w, q, \theta\}^T \quad (5.2)$$

While the control vector contains only elevators and ailerons deflection, neglecting throttle effects:

$$u = \{\delta_e, \delta_a\}^T \quad (5.3)$$

Therefore, A will be a $[4 \times 4]$ matrix and B a $[4 \times 2]$ matrix.

The characteristics of the longitudinal motion can be determined starting from aerodynamic forces and moments, expressed by mean of dimensional aerodynamic derivatives. Therefore, resolving in terms of accelerations, the system can be wrote as:

$$\begin{cases} \dot{u} = X_u u + X_w w - g \cos \theta \\ \dot{w} = \frac{Z_u}{1 - Z_{\dot{w}}} u + \frac{Z_w}{1 - Z_{\dot{w}}} w - \frac{g}{1 - Z_{\dot{w}}} \sin \theta + \frac{Z_q + V_0}{1 - Z_{\dot{w}}} q + \frac{Z_{\delta_e}}{1 - Z_{\dot{w}}} \delta_e + \frac{Z_{\delta_a}}{1 - Z_{\dot{w}}} 2\delta_a \\ \dot{q} = M_u u + M_w w + M_{\dot{w}} \dot{w} + M_q q + M_{\delta_e} \delta_e + M_{\delta_a} 2\delta_a \\ \dot{\theta} = q \end{cases} \quad (5.4)$$

In which V_0 is the initial aircraft speed and aileron deflections are multiplied by 2 as, in longitudinal dynamics, only their symmetrical deflection is considered. Substituting the second equation in the third equation, \dot{q} expression becomes:

$$\begin{aligned} \dot{q} = \left(M_u + \frac{M_{\dot{w}} Z_u}{1 - Z_{\dot{w}}} \right) u + \left(M_w + \frac{M_{\dot{w}} Z_w}{1 - Z_{\dot{w}}} \right) w + \left[M_q + \frac{M_{\dot{w}} (Z_q + V_0)}{1 - Z_{\dot{w}}} \right] q + \\ + \left(M_{\delta_e} + \frac{M_{\dot{w}} Z_{\delta_e}}{1 - Z_{\dot{w}}} \right) \delta_e + \left(M_{\delta_a} + \frac{M_{\dot{w}} Z_{\delta_a}}{1 - Z_{\dot{w}}} \right) 2\delta_a \quad (5.5) \end{aligned}$$

Rewriting the system in Eq. 5.4 substituting the third equation with Eq. 5.5 and assuming to have small perturbations, state and control matrices can be easily determined:

$$A = \begin{bmatrix} X_u & X_w & 0 & -g \\ \frac{Z_u}{1 - Z_{\dot{w}}} & \frac{Z_w}{1 - Z_{\dot{w}}} & \frac{Z_q + V}{1 - Z_{\dot{w}}} & 0 \\ M_u + \frac{M_{\dot{w}}Z_u}{1 - Z_{\dot{w}}} & M_w + \frac{M_{\dot{w}}Z_w}{1 - Z_{\dot{w}}} & M_q + \frac{M_{\dot{w}}(Z_q + V_0)}{1 - Z_{\dot{w}}} & 0 \\ 0 & 0 & 1 & 0 \end{bmatrix} \quad (5.6)$$

$$B = \begin{bmatrix} 0 & 0 \\ \frac{Z_{\delta_e}}{1 - Z_{\dot{w}}} & \frac{Z_{\delta_a}}{1 - Z_{\dot{w}}} \\ M_{\delta_e} + \frac{M_{\dot{w}}Z_{\delta_e}}{1 - Z_{\dot{w}}} & M_{\delta_a} + \frac{M_{\dot{w}}Z_{\delta_a}}{1 - Z_{\dot{w}}} \\ 0 & 0 \end{bmatrix} \quad (5.7)$$

The used derivatives, since the equations of motion are expressed in accelerations terms, are normalized with the aircraft mass for the aerodynamic forces and with the inertial tensor along the y axis for the aerodynamic moments. The derivatives of each state and command variable are reported below:

$$X_u = \frac{\rho SV_0}{2m} (-3C_{D_0}) \quad Z_u = \frac{\rho SV_0}{2m} (-2C_{L_0}) \quad M_u = \frac{\rho SV_0 \bar{c}}{2I_y} (C_{M_u}) \quad (5.8)$$

$$X_w = \frac{\rho SV_0}{2m} (C_{L_0}) \quad Z_w = \frac{\rho SV_0}{2m} (-C_{L_\alpha}) \quad M_w = \frac{\rho SV_0 \bar{c}}{2I_y} (C_{M_\alpha}) \quad (5.9)$$

$$Z_{\dot{w}} = \frac{\rho S \bar{c}}{4m} (-C_{L_{\dot{\alpha}}}) \quad M_{\dot{w}} = \frac{\rho S \bar{c}^2}{4I_y} (C_{M_{\dot{\alpha}}}) \quad (5.10)$$

$$Z_q = \frac{\rho SV_0 \bar{c}}{4m} (-C_{L_q}) \quad M_q = \frac{\rho SV_0 \bar{c}^2}{4I_y} (C_{M_q}) \quad (5.11)$$

$$Z_{\delta_e} = \frac{\rho SV_0^2}{2m} (-C_{L_{\delta_e}}) \quad M_{\delta_e} = \frac{\rho SV_0^2 \bar{c}}{2I_y} (C_{M_{\delta_e}}) \quad (5.12)$$

$$Z_{\delta_a} = \frac{\rho SV_0^2}{2m} (-C_{L_{\delta_a}}) \quad M_{\delta_a} = \frac{\rho SV_0^2 \bar{c}}{2I_y} (C_{M_{\delta_a}}) \quad (5.13)$$

However, in order to obtain a state-space definition of the system which can be used in the LQR controller design, matrices A and B in Eq. 5.6 and 5.7 must

be written in a non-dimensional form. Starting from non-dimensional forces and moments, these can be easily derived as follows:

$$\hat{F}_i = \frac{F_i}{\frac{1}{2}\rho V_0^2 S} \quad \hat{M}_i = \frac{M_i}{\frac{1}{2}\rho V_0^2 S \bar{c}} \quad (5.14)$$

In which, from now on, the superscript ($\hat{\cdot}$) indicates the non-dimensional form of the variable. The aircraft mass and the inertial tensor become:

$$\hat{m} = \frac{2m}{\rho S \bar{c}} \quad \hat{I}_y = \frac{I_y}{\rho S \left(\frac{\bar{c}}{2}\right)^3} \quad (5.15)$$

Finally, the time derivative in non dimensional form can be written as:

$$\frac{d}{dt} = \frac{2V_0}{\bar{c}} \quad (5.16)$$

Having these informations and knowing that the state-vector in its non-dimensional form is:

$$\hat{x} = \left\{ \frac{u}{V_0}, \frac{w}{V_0}, q \frac{\bar{c}}{2V_0}, \theta \right\}^T = \{\hat{u}, \alpha, \hat{q}, \theta\}^T \quad (5.17)$$

the state and control matrices become:

$$A = \begin{bmatrix} \frac{-3C_{D_0}}{2\hat{m}} & \frac{C_{L_0} - C_{D_\alpha}}{2\hat{m}} & 0 & -\frac{C_{W_e}}{2\hat{m}} \\ \frac{C_{L_0}}{2\hat{m} + C_{L_{\dot{\alpha}}}} & \frac{C_{L_\alpha} + C_{D_0}}{2\hat{m} + C_{L_{\dot{\alpha}}}} & \frac{2\hat{m}}{2\hat{m} + C_{L_{\dot{\alpha}}}} & 0 \\ -\frac{C_{M_{\dot{\alpha}}}}{2\hat{m} + C_{L_{\dot{\alpha}}}} & \frac{C_{M_\alpha} - C_{M_{\dot{\alpha}}}}{2\hat{m} + C_{L_{\dot{\alpha}}}} & \frac{C_{M_q} - C_{M_{\dot{\alpha}}}}{2\hat{m} + C_{L_{\dot{\alpha}}}} & 0 \\ \frac{\hat{I}_y}{0} & \frac{\hat{I}_y}{0} & \frac{\hat{I}_y}{1} & 0 \\ 0 & 0 & 1 & 0 \end{bmatrix} \quad (5.18)$$

$$B = \begin{bmatrix} 0 & 0 \\ \frac{C_{L_{\delta_e}}}{2\hat{m} + C_{L_{\dot{\alpha}}}} & -\frac{C_{L_{\delta_a}}}{2\hat{m} + C_{L_{\dot{\alpha}}}} \\ \frac{C_{M_{\delta_e}}}{\hat{I}_y} & \frac{C_{M_{\delta_a}}}{\hat{I}_y} \\ 0 & 0 \end{bmatrix} \quad (5.19)$$

In which the new derivatives C_{D_α} and C_{W_e} can be expressed as:

$$C_{D_\alpha} = \frac{2C_{L_\alpha}}{\pi e \frac{\bar{c}}{S}} C_{L_0} \quad C_{W_e} = \frac{mg}{\frac{1}{2}\rho V_0^2 S} \quad (5.20)$$

5.2 Linear Quadratic Regulator (LQR)

Once the the state space system is defined, it is possible to proceed with the LQR design. The LQR is a technique that provides optimal controllers through a mathematical algorithm that minimizes a cost function with weighting factors defined by the user. In other words, the LQR algorithm is an automated way to find an appropriate state-feedback controller K that minimizes a cost function J which includes the deviation of key measurements from their desired values and the magnitude of control action needed.

Therefore, in general the optimal LQR problem consists of finding the control input that minimizes:

$$J = \int_0^{\infty} x^T Q x + \rho u^T R u dt \quad (5.21)$$

With ρ positive constant and Q and R symmetric positive-definite matrices. These are respectively the weighting matrices associated to the states and the commands. It can be noticed that greater values of Q elements would lead to a great state alleviation at the cost of a large control input, while grater values of R elements would lead to controller which generates small control input but large control output.

In this thesis Q is selected as an identity matrix $Q = I^{4 \times 4}$, while R is selected as diagonal matrix in which the elements are computed by means of the Bryson's rule [32] (ρ is taken as unitary):

$$R_{jj} = \frac{1}{\text{maximum acceptable value of } u_j^2} \quad \text{with } j = 1, \dots, N \quad (5.22)$$

Therefore, in matrix form:

$$R = \begin{bmatrix} 1 & 0 \\ |\delta_{e_{MAX}}|^2 & \\ 0 & 1 \\ & |\delta_{a_{MAX}}|^2 \end{bmatrix} \quad (5.23)$$

In practice, the Bryson's rule scales the variables so that the maximum acceptable value of each term is one. This is important especially when the units used for different components of the command (and/or state) vector make the values of these variables numerically different from each other [31]. However, Bryson's rule its also often used as starting point of a trial-and-error process aimed to obtain the desired closed-loop performance.

The aim of the LQR controller is to find a control input u the minimizes the cost function J in Eq. 5.21. As stated before, this could be done by means of a state-feedback K for which the optimal control is given by:

$$u = -Kx \tag{5.24}$$

In which K is defined as:

$$K = R^{-1}B^T P \tag{5.25}$$

Where P is a symmetric matrix obtained from the resolution of the Algebraic Ricatti Equation (ARE):

$$A^T P + PA + Q - PBR^{-1}B^T P = 0 \tag{5.26}$$

This equation is used since the LQR problem can be solved using an argument based on "square completion" that avoids the use of calculus of variations. This means the the problem is rewritten dividing Eq. 5.21 in two terms:

$$J = J_0 + \int_0^\infty (u(t) - u_0(t))^T R (u(t) - u_0(t)) dt \tag{5.27}$$

In witch J_0 is called "feedback invariant" and, by definition, its value does not depend on the choice of the control input. It can be demonstrated that this definition of the problem can be achieved by introducing a symmetric matrix P which can be found by solving Eq. 5.26. Solving the problem in this form leads to definition of the feedback matrix K as given in Eq. 5.25.

In practice the LQR control design can be summarized in three steps:

- Definition of the weighting matrices Q and R .
- Resolution of the ARE (Eq. 5.26) to find the matrix P .
- Computation of the gain matrix K as defined in Eq. 5.25.

Since the considered state vector has four elements and the control vector contains elevator and aileron deflections, in this case K is a $[2 \times 4]$ matrix. The obtained closed loop is schematized in Figure 5.1.

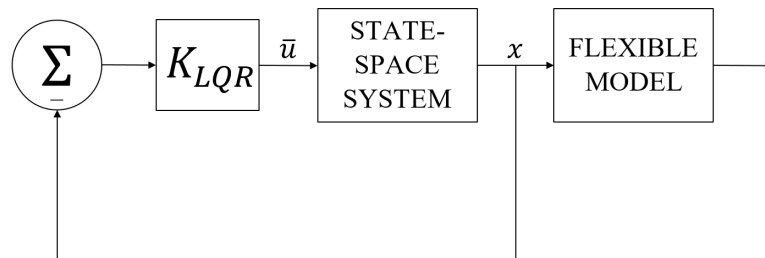


Figure 5.1: Closed Loop System Scheme

5.3 Control System Implementation

Implementing an LQR controller on the rigid model means not only controlling and reducing the gust loads acting on the flexible wing but also, clearly, improving the aircraft dynamics characteristics. Particularly, since in this case only the longitudinal dynamics were considered, phugoid and short period will be affected. Once the loop is closed with the gain matrix obtained in Eq. 5.25, as shown in Figure 5.1, the new resulting system can be rewritten as:

$$\dot{x} = (A - KB)x + Bu \quad (5.28)$$

In which $(A - KB)$ is the closed loop state matrix. Computing the eigenvalues of both open and closed loop matrices and plotting the results on the complex plane leads to the graph shown in Figure 5.2. From the graph it is clear how the LQR controller as defined in Section 5.2 has a great impact on the aircraft dynamics, stabilizing both the phugoid and the short period modes.

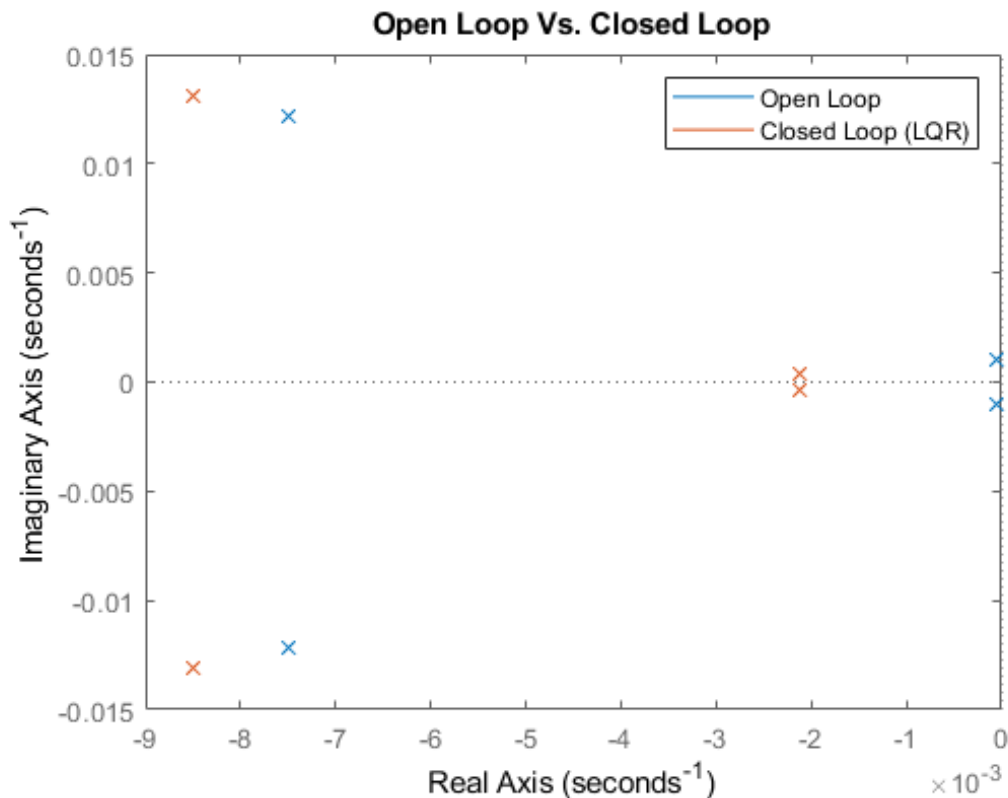


Figure 5.2: Open Loop Vs. Closed Loop Eigenvalues

Also its visible how the LQR tends to completely cancel the phugoid by reducing its imaginary part. Its possible to improve the control action by modifying weight matrices Q and R or the gain ρ , but this also leads to a stronger response of the aircraft, thus reducing the comfort of the passengers. For this reason, weights and ρ were left to the initial values reported in Table 5.1.

LQR Controller Data	
ρ	1
$\delta_{e_{MAX}}$	$\pm 15^\circ$
$\delta_{a_{MAX}}$	$\pm 10^\circ$

Table 5.1: LQR Controller Data

The main objective of the controller designed in this section is to reduce the loads induced by a gust on the flexible wing structure. The analysed perturbations are the discrete "1 – cos" gust (Figure 4.5) and the von Kármán moderate turbulence (Figure 4.8) presented in Chapter 4. The chosen load determination method is the one based on the MCK form of the flexible system, since it is the most accurate between the two methods presented in this work. All the external perturbations were started after 4 seconds of simulation, in order to start at an equilibrium state.

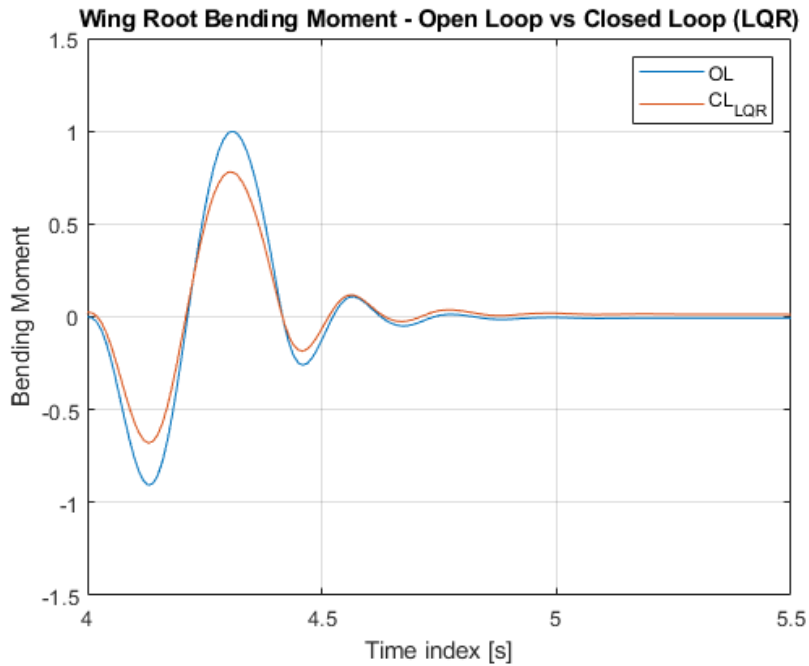


Figure 5.3: Open Loop Vs. Closed Loop - Bending Moment - "1 – cos" Discrete Gust

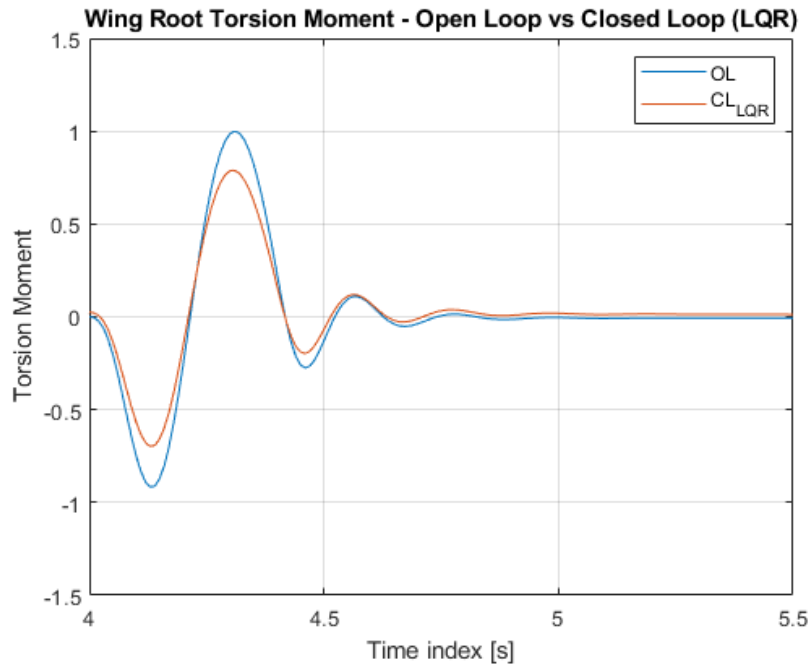


Figure 5.4: Open Loop Vs. Closed Loop - Torsion Moment - "1 – cos" Discrete Gust

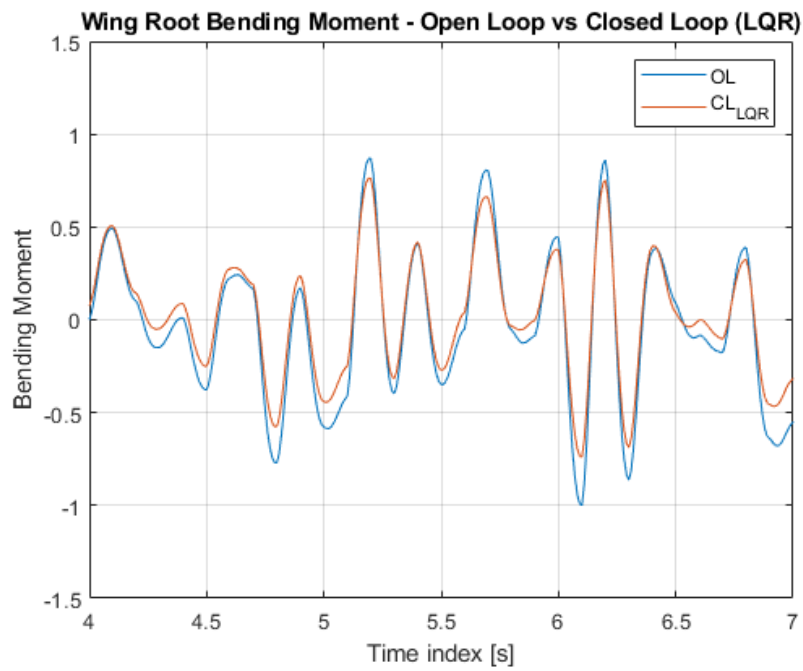


Figure 5.5: Open Loop Vs. Closed Loop - Bending Moment - von Kármán Gust

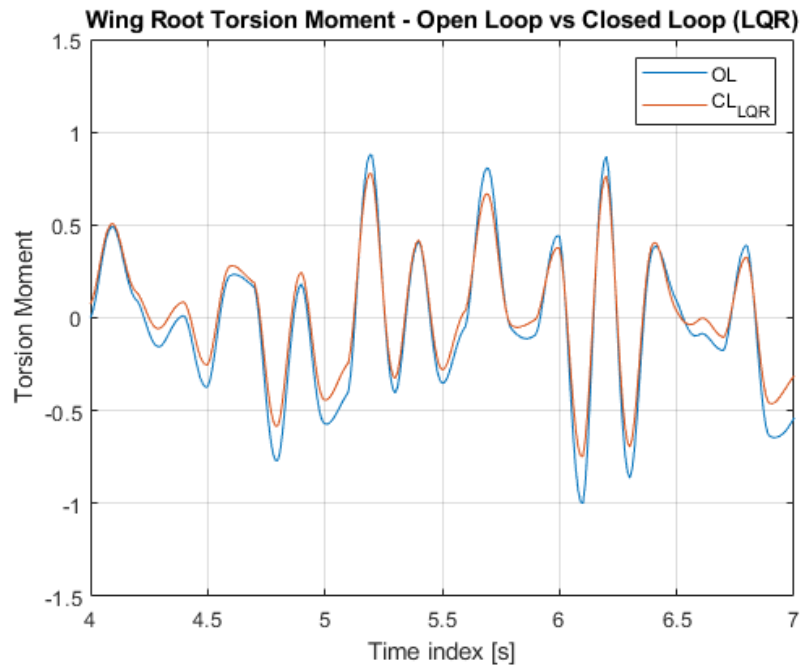


Figure 5.6: Open Loop Vs. Closed Loop - Torsion Moment - von Kármán Gust

Figures 5.3 and 5.4 show the comparison between open loop and closed loop loads after a discrete gust has perturbed the aircraft, while Figures 5.5 and 5.6 show the effect of the controller after a von Kármán continuous gust.

These graphs show how the implementation of an LQR on the rigid body dynamics leads to an effective load reduction both in terms of bending and torsion moments. The reduction at the maximum peak for the discrete "1 – cos" gust is about 22% for the bending moment and about 21% for the torsion moment.

The results for the von Kármán moderate turbulence, although the load reduction is clearly visible, are a little less consistent if compared to the discrete gust. This is imputable to multiple factors: for example the rapid changes in velocity direction do not permit the model to update accordingly to the command action, and thus, especially for the small peaks, it's visible a small translation of the loads instead of a proper reduction. Also, in general, peak velocities of a continuous gust are small if compared with the discrete gust ones. This translates in smaller command amplitude and therefore in a smaller effect on the loads which is heavily influenced by the sensitivity of the entire system to the control action. In any case, the maximum reduction reached at peak for the von Kármán turbulence is of 26% for the bending moment and 25% for the torsion moment, with an average reduction at the peaks, for both the moments, of about 15%.

Chapter 6

Conclusions

This thesis aims to give a complete overall on the simulation of a flexible aircraft, especially for what is concerning dynamic wing loads in an unsteady atmospheric condition, and their reduction via an optimal control technique.

Chapter 2 shows how the presented flexible model maintains a strong link with the rigid dynamics model. For this reason the implementation in Matlab/Simulink of the model results to be very practical, since it is possible to simulate firstly the rigid aircraft dynamics and then use the rigid states to implement the flexible model via the Lagrangian approach. Also, expressing the obtained set of equations by means of generalized coordinates using the Galérkin method, reduces the complexity of the formulation and thus the computational load required. Furthermore, the external aerodynamic forces can be expressed as sum of a "frozen" component and an increment generated by the deformation rates. This permits to consider the effect of the aerodynamic damping by expressing the latter component of the generalized forces by means of the Rayleigh dissipation function.

Since a strong link is maintained between rigid and flexible aircraft models, the flexible wing response to a gust can be evaluated by simply implementing the turbulence models presented in Chapter 3 directly as wind perturbation inside the rigid dynamics model. This is possible since both the presented discrete and continuous models express the gust as a wind velocity component time history, which can be easily summed to the velocity components of the state vector. The resulting velocities are then used inside the Lagrange's equations and thus the elastic response of the structure to the selected gust can be evaluated.

Chapter 4 shows wing response and the load generated by the external gusts. In particular, speaking of the load determination methods, it is clear how the method based on the strip theory as produced greater loads than the one based directly on the MCK formulation of the flexible system. Such behaviour is visible in the bending loads (5-13% increment) but is greatly accentuated for torsional loads (~20% increment). This happens, as already stated before, because the method neglects

some structural damping terms which are instead contained in the flexible system equations. This could be acceptable for data collection or for some structural applications, but it is not suitable for the control law design. Greater loads, in fact, could induce the control engineer to set an unnecessary great control action which can result in both degradation of the flight quality and passenger comfort. On the other hand, the MCK method necessarily requires the definition of a flexible model and, thus, some data obtained with previous structural analyses. This does not represent a problem for simulation purposes, but may be unpractical if the objective is to evaluate the loads during air tunnel tests or just for data collection. For this reason both of the methods are presented in this thesis.

In any case, the load determination method based on the MCK formulation is the one selected to evaluate the effectiveness of the control law implemented in Chapter 5. The LQR controller results to be very effective for both stabilizing the aircraft response and for the load alleviation, especially thanks to the combined action of elevator and the symmetric activation of the ailerons. The drawback of this implementation is that the controller acts on the aircraft attitude without acting directly on the wing deformation. This could result sometimes in a controller limitation in order to not compromise, for example, the passengers comfort. Also, for the continuous turbulence loads, it is clear that the entire aircraft response to the control input is not always on point with the load reduction. On the other hand, the LQR controller leads to good results in both aircraft response and load alleviation, with an average load reduction of the 20%, with minimum implementation effort. In fact the model configuration, makes easy to implement the feedback controller in terms of gain K , directly inside the real time simulation. Therefore, also the comparison between the open loop and closed loop loads, obtained with the methods presented in Chapter 4 is straightforward.

It is clear now that the strength of this model is the ease with it is possible to implement new parts, depending on what is required, without burdening too much the formulation. This results in a great advantage in early design phases, although further steps in an aircraft development may require more accurate analyses, especially for what is concerning the structural studies. However, the model is also well predisposed for being updated with more accurate structural data coming from a FEM analyses as, for example, shape functions of high order modes. This makes it a good instrument to study flexible aircraft dynamics and for control law design and testing.

Concluding, although some approximations have been made, the model presented in this thesis, represents a good foundation for an accurate and complete analysis of the flexible aircraft dynamics in a turbulent atmosphere for real time simulation and gust load alleviation purposes.

6.1 Future Developments

This section aims to suggest some possible future improvements for each part of the presented study, especially for the aircraft modelling, load determination and control design sections.

In future implementations the presented model could be improved considering the complete rigid aircraft dynamics and including other flexible parts in additions to the wings, such as the fuselage and the tail. Also the aerodynamic loads could be calculated non only by means of local variation of the angle of attack, but including the contribution of control surfaces, as ailerons, on the interested sections. This could lead to a better representation of the effects commands have on the flexible loads, especially for gust load alleviation purposes. Other possible developments could include higher bending and torsional modes, in order to evaluate which is the best compromise between result accuracy and computational load. Also, aeroelastic effects such as flutter, buffering, divergence and control surface reversal could be studied starting from the presented flexible model.

Regarding the load determination methods, as already stated before, while the strip theory method could lead in some cases to an excessive approximation, the MCK method requires some structural data which is available only through previous structural analyses. A solution in between of the two presented in this work, could be the definition of method based on a fine aerodynamic mesh, in order to obtain an accurate load determination knowing only part of the structural data.

Finally, concerning the control law design, in future developments it can be evaluated the use of two combined controllers, one for the rigid dynamics and one specifically designed for the flexible dynamics. This could be done by means of, for example, a FIR filter or more robust controllers, like \mathcal{L}_1 or \mathcal{H}_∞ which could achieve not only a good load reduction but also load control.

Appendices

Appendix A

Complete Non-Linear Rigid Aircraft Model

As already stated in Section 2.1, the rigid model is based on the non-linear dimensional equations of motion written in the body axes frame as reported in [26]. The resulting 6 DoF differential equation system takes in consideration 12 variables, that are:

- Linear velocities $\{u, v, w\}$, from force equations.
- Angular rates $\{p, q, r\}$, from moment equations.
- Euler angles $\{\phi, \theta, \psi\}$, from kinematic equations.
- Coordinates $\{x_N, y_E, z_D\}$, from navigation equations (NED reference frame).

Force equations are classically expressed directly in terms of linear accelerations, as reported in the following matrix form:

$$\begin{pmatrix} \dot{u} \\ \dot{v} \\ \dot{w} \end{pmatrix} = - \begin{bmatrix} 0 & -r & q \\ r & 0 & -p \\ -q & p & 0 \end{bmatrix} \begin{pmatrix} u \\ v \\ w \end{pmatrix} + \frac{g}{W} \begin{pmatrix} X \\ Y \\ Z \end{pmatrix} \quad (\text{A.1})$$

Where X , Y and Z represent the aerodynamic forces along the body axes, g is the the gravitational acceleration and W is the aircraft weight. In a similar fashion, moment equations are expressed as follows;

$$\begin{pmatrix} \dot{p} \\ \dot{q} \\ \dot{r} \end{pmatrix} = [I_B]^{-1} \left(\begin{pmatrix} \mathbb{L} \\ \mathbb{M} \\ \mathbb{N} \end{pmatrix} - \begin{bmatrix} 0 & -r & q \\ r & 0 & -p \\ -q & p & 0 \end{bmatrix} [I_B] \begin{pmatrix} p \\ q \\ r \end{pmatrix} \right) \quad (\text{A.2})$$

In which \mathbb{L} , \mathbb{M} and \mathbb{N} are the aerodynamic moments in body axes reference frame and I_B is the inertial tensor, in general defined as:

$$[I_B] = \begin{bmatrix} I_{xx} & -I_{xy} & -I_{xz} \\ -I_{xy} & I_{yy} & -I_{yz} \\ -I_{xz} & -I_{yz} & I_{zz} \end{bmatrix} \quad (\text{A.3})$$

Figure A.1 gives a representation of the body reference frame, including linear velocities, angular rates and aerodynamic forces and moments.

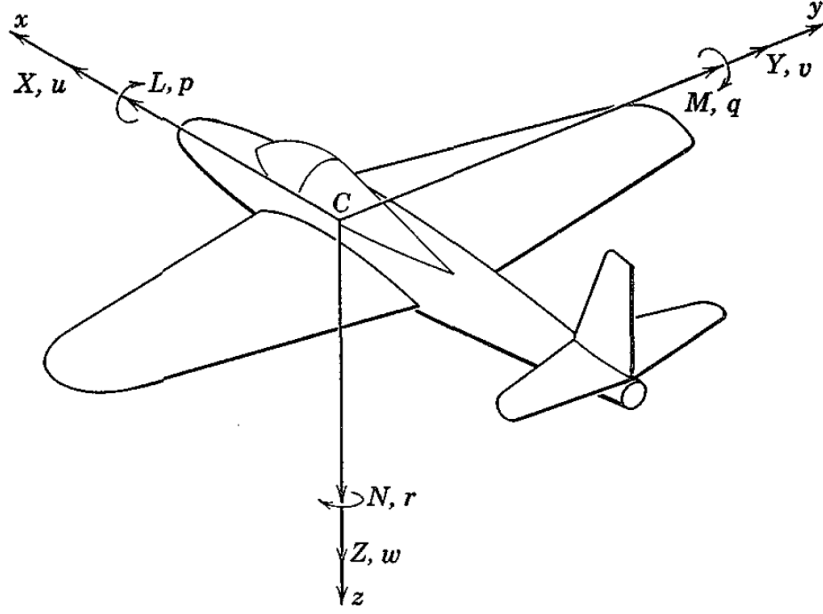


Figure A.1: Body Axes Reference Frame

Continuing with the rigid model definition, kinematic equations used to obtain the Euler angles are defined as:

$$\begin{Bmatrix} \dot{\phi} \\ \dot{\theta} \\ \dot{\psi} \end{Bmatrix} = \begin{bmatrix} 1 & \frac{S_\phi \cdot S_\theta}{C_\theta} & \frac{C_\phi \cdot S_\theta}{C_\theta} \\ 0 & C_\phi & -S_\phi \\ 0 & \frac{S_\phi}{C_\theta} & \frac{C_\phi}{C_\theta} \end{bmatrix} \begin{Bmatrix} p \\ q \\ r \end{Bmatrix} \quad (\text{A.4})$$

Where $S_{(\cdot)}$ and $C_{(\cdot)}$ are respectively sine and cosine functions. Finally position coordinates in NED reference frame can be determined by means of navigation equations:

$$\begin{Bmatrix} \dot{X}_N \\ \dot{Y}_E \\ \dot{Z}_D \end{Bmatrix} = \begin{bmatrix} C_\theta \cdot C_\psi & S_\phi \cdot S_\theta \cdot C_\psi - C_\phi \cdot S_\psi & C_\phi \cdot S_\theta \cdot C_\psi + S_\phi \cdot S_\psi \\ C_\theta \cdot S_\psi & S_\phi \cdot S_\theta \cdot S_\psi + C_\phi \cdot C_\psi & C_\phi \cdot S_\theta \cdot S_\psi - S_\phi \cdot C_\psi \\ -S_\theta & S_\phi \cdot C_\theta & C_\phi \cdot C_\theta \end{bmatrix} \begin{Bmatrix} u \\ v \\ w \end{Bmatrix} \quad (\text{A.5})$$

In order to conclude the rigid model definition, aerodynamic forces and moments must be defined. Aerodynamic forces acting on the aircraft can be seen as sum of three contributions:

$$X = X_G + X_A + X_T \quad (\text{A.6})$$

$$Y = Y_G + Y_A + Y_T \quad (\text{A.7})$$

$$Z = Z_G + Z_A + Z_T \quad (\text{A.8})$$

Where subscripts G , A and T represent respectively gravitational, aerodynamic and thrust forces. Gravitational terms can be simply defined as:

$$X_G = -mg \sin \theta \quad (\text{A.9})$$

$$Y_G = mg \sin \phi \cos \theta \quad (\text{A.10})$$

$$Z_G = mg \cos \phi \cos \theta \quad (\text{A.11})$$

In which m is the aircraft mass. Aerodynamic forces, instead, are expressed as:

$$X_A = -D \cos \alpha + L \sin \alpha \quad (\text{A.12})$$

$$Y_A = Y \quad (\text{A.13})$$

$$Z_A = -D \sin \alpha - L \cos \alpha \quad (\text{A.14})$$

Where L , D and Y represent respectively lift, drag and side force. Assuming the thrust force equal to drag in magnitude and direction, but of opposite sign, the total forces can be expressed as:

$$X = -D \cos \alpha + L \sin \alpha - mg \sin \theta + (D \cos \alpha)_T \quad (\text{A.15})$$

$$Y = Y + mg \sin \phi \cos \theta \quad (\text{A.16})$$

$$Z = -D \sin \alpha - L \cos \alpha + mg \cos \phi \cos \theta + (D \sin \alpha)_T \quad (\text{A.17})$$

The aerodynamic forces (L , D , Y) and moments (\mathbb{L} , \mathbb{M} , \mathbb{N}) can be derived by the following classical equations:

$$L = \frac{1}{2} \rho V^2 S C_L \quad (\text{A.18})$$

$$D = \frac{1}{2} \rho V^2 S C_D \quad (\text{A.19})$$

$$Y = \frac{1}{2} \rho V^2 S C_Y \quad (\text{A.20})$$

$$\mathbb{L} = \frac{1}{2} \rho V^2 S b C_l \quad (\text{A.21})$$

$$\mathbb{M} = \frac{1}{2} \rho V^2 S \bar{c} C_m \quad (\text{A.22})$$

$$\mathbb{N} = \frac{1}{2} \rho V^2 S b C_n \quad (\text{A.23})$$

In which ρ is the air density, V is the aircraft speed, b is the wing span and \bar{c} is the mean aerodynamic chord. The aerodynamic coefficients are calculated using classical flight mechanics linear expressions:

$$C_L = C_{L_0} + C_{L_\alpha} \alpha + \left(C_{L_\dot{\alpha}} \dot{\alpha} + C_{L_q} q \right) \frac{\bar{c}}{V} + C_{L_{\delta_e}} \delta_e + C_{L_{\delta_a, SYMM}} (\delta_{a_R} + \delta_{a_L}) \quad (\text{A.24})$$

$$C_D = C_{D_0} + k C_L^2 + C_{D_{\delta_a, SYMM}} (\delta_{a_R} + \delta_{a_L}) \quad (\text{A.25})$$

$$C_Y = C_{Y_\beta} \beta + \left(C_{Y_p} p + C_{Y_r} r \right) \frac{b}{V} + C_{Y_{\delta_r}} \delta_r + C_{Y_{\delta_a}} \left(\frac{\delta_{a_R} + \delta_{a_L}}{2} \right) \quad (\text{A.26})$$

$$C_l = C_{l_\beta} \beta + \left(C_{l_p} p + C_{l_r} r \right) \frac{b}{V} + C_{l_{\delta_r}} \delta_r + C_{l_{\delta_a}} \left(\frac{\delta_{a_R} + \delta_{a_L}}{2} \right) \quad (\text{A.27})$$

$$C_M = C_{M_0} + C_{M_\alpha} \alpha + \left(C_{M_\dot{\alpha}} \dot{\alpha} + C_{M_q} q \right) \frac{\bar{c}}{V} + C_{M_{\delta_e}} \delta_e \quad (\text{A.28})$$

$$C_n = C_{n_\beta} \beta + \left(C_{n_p} p + C_{n_r} r \right) \frac{b}{V} + C_{n_{\delta_r}} \delta_r + C_{n_{\delta_a}} \left(\frac{\delta_{a_R} + \delta_{a_L}}{2} \right) \quad (\text{A.29})$$

Note that derivatives with subscripts $\delta_{a, SYMM}$ are referred to the symmetric activation of the ailerons. The airspeed V , the angle of attack α and the side-slip angle β are proper of the wind axes, therefore they need to be expressed in body axes as follows:

$$V = \sqrt{u^2 + v^2 + w^2} \quad (\text{A.30})$$

$$\alpha = \arctan \frac{w}{u} \quad (\text{A.31})$$

$$\beta = \arcsin \frac{v}{V} \quad (\text{A.32})$$

The last term needed to complete the aerodynamic forces determination is $\dot{\alpha}$, which can be derived by manipulating the linear velocities and their respective rates:

$$\dot{\alpha} = \frac{u\dot{w} - \dot{u}w}{u^2 + w^2} \quad (\text{A.33})$$

Bibliography

- [1] C.-S. Chang, D. H. Hodges, and M. J. Patil, “Flight Dynamics of Highly Flexible Aircraft,” *Journal of Aircraft*, vol. 45, pp. 538–545, Mar. 2008.
- [2] J. L. Junkins and Y. Kim, *Introduction to dynamics and control of flexible structures*. AIAA education series, Washington, D.C: American Institute of Aeronautics and Astronautics, 1993.
- [3] E. H. Dowell, *A Modern Course in Aeroelasticity*. Cham: Springer International Publishing, 2015.
- [4] R. Milne, *Dynamics of the Deformable Aeroplane*. Queen Mary College, London: Her Majesty’s Stationery Office Reports and Memoranda Rept. 3345, 1964.
- [5] R. K. Cavin and A. R. Dusto, “Hamilton’s principle - Finite-element methods and flexible body dynamics,” *AIAA Journal*, vol. 15, pp. 1684–1690, Dec. 1977.
- [6] C. Buttrill, P. Arbuckle, and T. Zeiler, “Nonlinear simulation of a flexible aircraft in maneuvering flight,” in *Flight Simulation Technologies Conference*, (Monterey, CA, U.S.A.), American Institute of Aeronautics and Astronautics, Aug. 1987.
- [7] L. Meirovitch and I. Tuzcu, “Unified Theory for the Dynamics and Control of Maneuvering Flexible Aircraft,” *AIAA Journal*, vol. 42, pp. 714–727, Apr. 2004.
- [8] G. Avanzini, E. Capello, and I. A. Piacenza, “Mixed Newtonian–Lagrangian Approach for the Analysis of Flexible Aircraft Dynamics,” *Journal of Aircraft*, vol. 51, pp. 1410–1421, Sept. 2014.
- [9] EASA, “Certification Specifications and Acceptable Means of Compliance for Large Aeroplanes CS-25 - Amendment 23,” July 2019.
- [10] F. M. Hoblit, *Gust loads on aircraft: concepts and applications*. AIAA education series, Washington, D.C: American Institute of Aeronautics and Astronautics, 1988.
- [11] H. W. Liepmann, “On the Application of Statistical Concepts to the Buffeting Problem,” *Journal of the Aeronautical Sciences*, vol. 19, pp. 793–800, Dec. 1952.
- [12] T. de Karman and L. Howarth, “On the Statistical Theory of Isotropic Turbulence,” *Proceedings of the Royal Society of London. Series A - Mathematical*

- and Physical Sciences*, vol. 164, pp. 192–215, Jan. 1938.
- [13] U. S. Department of Defense, “Flying Qualities of Piloted Aircraft - U.S. Military Handbook MIL-HDBK-1797,” Dec. 1997.
 - [14] D. McLean, “Gust-alleviation control systems for aircraft,” *Proceedings of the Institution of Electrical Engineers*, vol. 125, no. 7, p. 675, 1978.
 - [15] P. Roesch and R. Harlan, “A passive gust alleviation system for light aircraft,” in *Mechanics and Control of Flight Conference*, (Anaheim, CA, U.S.A.), American Institute of Aeronautics and Astronautics, Aug. 1974.
 - [16] S. Guo, J. De Los Monteros, and Y. Liu, “Gust Alleviation of a Large Aircraft with a Passive Twist Wingtip,” *Aerospace*, vol. 2, pp. 135–154, Apr. 2015.
 - [17] Y. Tani, S. Seki, and S. Aso, “An Experimental Study on Gust Load Alleviation using Passive Ventilation Wing Concept,” in *2018 AIAA Aerospace Sciences Meeting*, (Kissimmee, Florida), American Institute of Aeronautics and Astronautics, Jan. 2018.
 - [18] J. Zeng, B. Moulin, R. de Callafon, and M. J. Brenner, “Adaptive Feedforward Control for Gust Load Alleviation,” *Journal of Guidance, Control, and Dynamics*, vol. 33, pp. 862–872, May 2010.
 - [19] S. S. Haykin, *Adaptive filter theory*. Upper Saddle River, New Jersey: Pearson, fifth edition ed., 2014.
 - [20] M. Dillsaver, C. Cesnik, and I. Kolmanovsky, “Gust Load Alleviation Control for Very Flexible Aircraft,” in *AIAA Atmospheric Flight Mechanics Conference*, (Portland, Oregon), American Institute of Aeronautics and Astronautics, Aug. 2011.
 - [21] K. Zhou, J. C. Doyle, and K. Glover, *Robust and optimal control*. Upper Saddle River, N.J: Prentice Hall, 1996.
 - [22] P. J. Gonzalez, F. J. Silvestre, P. Paglione, A. Köthe, Z. Y. Pang, and C. E. Cesnik, “Linear Control of Highly Flexible Aircraft based on Loop Separation,” in *AIAA Atmospheric Flight Mechanics Conference*, (Washington, D.C.), American Institute of Aeronautics and Astronautics, June 2016.
 - [23] N. Aouf, B. Boulet, and R. Botez, “H/sub 2/ and H/sub /spl infin// -optimal gust load alleviation for a flexible aircraft,” in *Proceedings of the 2000 American Control Conference. ACC (IEEE Cat. No.00CH36334)*, (Chicago, IL, USA), pp. 1872–1876 vol.3, IEEE, 2000.
 - [24] R. G. Cook, R. Palacios, and P. Goulart, “Robust Gust Alleviation and Stabilization of Very Flexible Aircraft,” *AIAA Journal*, vol. 51, pp. 330–340, Feb. 2013.
 - [25] E. Capello, G. Guglieri, and F. Quagliotti, “A Comprehensive Robust Adaptive Controller for Gust Load Alleviation,” *The Scientific World Journal*, vol. 2014, pp. 1–12, 2014.
 - [26] B. Etkin, *Dynamics of atmospheric flight*. Mineola, N.Y.: Dover Publications,

- 2005.
- [27] L. Meirovitch, *Principles and techniques of vibrations*. Upper Saddle River, N.J: Prentice Hall, 1997.
 - [28] MATLAB Aerospace Blockset Documentation, *Dryden Wind Turbulence Model (Continuous)*. Natick, Massachusetts: The MathWorks, Inc., 2019. Available on: <https://it.mathworks.com/help/aeroblks/drydenwindturbulencemodelcontinuous.html>.
 - [29] MATLAB Aerospace Blockset Documentations, *Von Karman Wind Turbulence Model (Continuous)*. Natick, Massachusetts: The MathWorks, Inc., 2019. Available on: <https://it.mathworks.com/help/aeroblks/vonkarmanwindturbulencemodelcontinuous.html>.
 - [30] C. Casarosa, *Meccanica del volo*. Pisa: Pisa University Press, 2013.
 - [31] J. P. Hespanha, *Lecture Notes on LQR/LQG Controller Design , Knowledge Creation Diffusion Utilization*. 2005.
 - [32] G. F. Franklin, J. D. Powell, and A. Emami-Naeini, *Feedback control of dynamic systems*. Upper Saddle River, N.J: Pearson Prentice Hall, 5th ed., 2006.